SIMULATING HUBBLE XDF OBSERVATIONS FOR THE NEXT GENERATION OF SPACE TELESCOPES

by

Martin Hellmich

A THESIS SUBMITTED IN PARTIAL FULFILMENT OF
THE REQUIREMENTS FOR THE DEGREE OF

BACHELOR OF SCIENCE

in

Honours Astrophysics

(Department of Astronomy and Physics, Dr. Marcin Sawicki supervising faculty)

....

....

....

....

....

SAINT MARY'S UNIVERSITY

April 30, 2019

© Martin Hellmich, 2019

Abstract

Simulating Hubble XDF observations for the next generation of
space telescopes.

by *Martin Hellmich*

submitted on April 30, 2019:

This research created spatially resolved exposure simulations for 4457 galaxies in the eXtreme Deep Field for CASTOR and WFIRST and Euclid bandwidths. This next generation of space based observatories will improve on Hubble and GALEX observations in depth, bandwidth range and survey area. The Cosmological Advanced Survey Telescope for Optical and ultraviolet Research (CASTOR), currently in the design study phase, is a proposed mission in ultraviolet and optical bands. It will cover a large survey field while improving on resolution and sensitivity of its predecessor GALEX. CASTOR observations will be complimentary to NASA's Wide-Field Infrared Survey Telescope (WFIRST) and ESA's Euclid spacecraft. By investigating the information that these simulations provide, insight is gained into the possible performance of the observatories. A noise simulation was developed for CASTOR bandwidths and compared to WFIRST sensitivities in its bandwidths. From a comparison of proposed CASTOR filters it was found that the G, U and UV filters produce the best SNR. A selection of galaxies spanning a range of magnitudes from 22-27 (F140W AB) and range of redshifts from 0.5-2.0 were examined. It was found that for objects

approaching redshifts of 2.0 and magnitudes of 27 it will be difficult to do research involving spatially resolved SED fitting with 100 hour observations. While for objects with a redshifts of 0.5-1.5 and magnitudes of 22-24, 100 hour observations provide excellent SNR. Further, similar results will be achieved in 10 hour observations by WFIRST in its IR bandwidths.

Contents

List of Figures

List of Tables

Chapter 1

INTRODUCTION

1.1 GALAXY EVOLUTION

The study of galaxy evolution is about the history and eventual fate of habitable corners of the universe. Our Galaxy is our heritage and understanding its origin is an important piece of our story as well as the story of the universe. The night sky provides us with a large and varied assortment of galaxies throughout the universe in both space and time. The photons from these galaxies cary clues about the conditions in the universe from when our Galaxy was just forming, to all the way back shortly after the Big Bang.

Understanding the evolution of galaxies involves studying stellar and dust distribution and star formation history. Such information can be derived by fitting stellar population models to observed magnitudes in multiple wavelengths (Sawicki, 2012). It is important to observe a sufficient portion of the electromagnetic spectrum to have an accurate understanding of stellar processes in galaxies. Space observatories have led the path to making such studies possible. From unprecedented depth and clarity of images to unleashing exploration into bandwidths invisible from Earth the Hubble Space Telescope (HST), and its space-based contemporaries have set the path for

further innovation to reach ever deeper into the universe.

The Ultra Violet (UV) portion of the spectrum has special significance for galaxy evolution. It is from hot, young, and short lived stars that we observe UV emission so UV emission is a identifier for star formation (Côté, 2018). It also allows the use of the Lyman break technique to distinguish between high and low redshift galaxies (Steidel et al., 1996). The Galaxy Evolution Explorer (GALEX) was an orbiting UV telescope that operated from 2003 to 2013 (Martin et al., 2019). GALEX enabled studies of star formation history, galaxy spectral energy distributions (SED's), and photometric redshifts (e.g., Williams et al. (2010), Kartaltepe et al. (2010)). Future space telescope designs must balance resources to make sure they are properly equipped to continue the work done with GALEX and HST.

1.2 CASTOR

The Cosmological Advanced Survey Telescope for Optical and ultraviolet Research (CASTOR), see figure 1.1, is a proposed Canadian-led mission currently under investigation by a CSA-funded consortium of universities and industrial labs. The telescope will improve on resolution and sensitivity in UV and optical bands compared to GALEX. The observed bandwidth will cover 150-550 nm, in five filters (Côté, 2018). CASTOR will have a 1.0 m aperture giving it a resolution of 0.15", an improvement of a factor of 30 over GALEX (Côté, 2018). A wide 1.16° x 0.58° field of view will be used to cover large survey area during the telescopes operation (Côté et al., 2012). Figure 1.2 shows the comparison between CASTOR and HST fields of view.
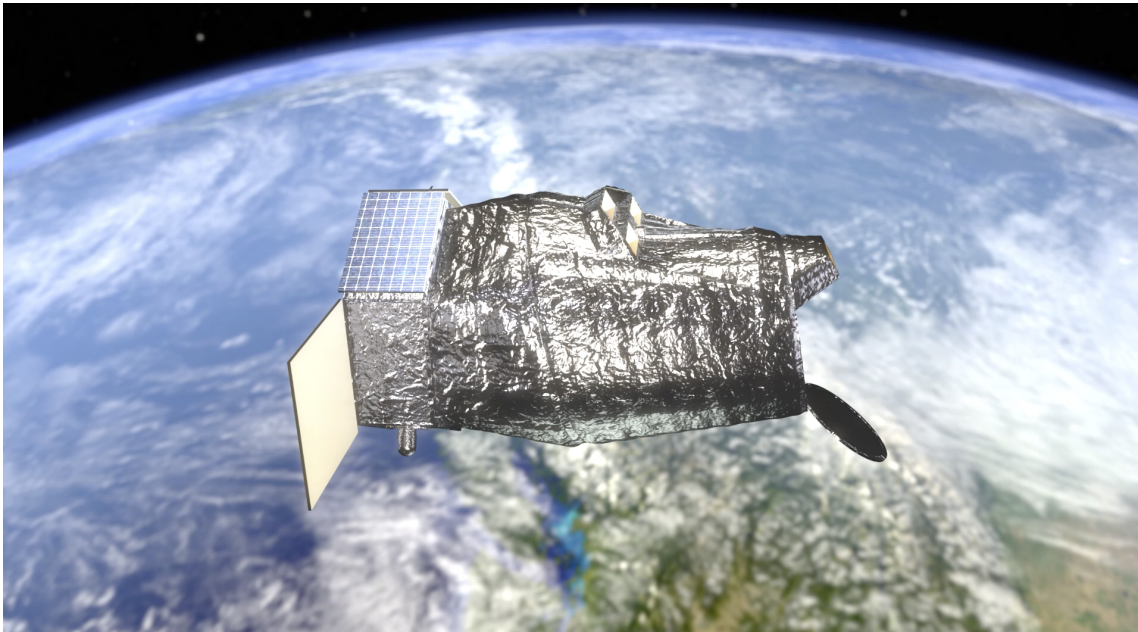
Figure 1.1: Artist concept of CASTOR. Figure from Côté et al. (2019), used with permission.

CASTOR is capable of several proposed surveys. One important example is Wide Survey. This survey would image 1/8 of the sky to a U-band depth of 27.1 mag (Côté et al., 2012). Other Surveys include the Deep (Ulim=29.8), Nearby Galaxies, and Nearby Clusters surveys. The observations are targeted to suit investigations of a wide variety of topics including: dark energy, cosmology, galaxy evolution, stellar and planetary and outer solar system.

The primary importance of CASTOR to studies of galaxy evolution is the improvement in depth and resolution of observations in the UV. Along with similarly improved observations from WFIRST and Euclid in IR bandwidths, SED fitting will be possible with greater accuracy and spatial resolution.Through SED fitting with modelled galaxy spectra, parameters such as stellar mass and star formation are extracted (e.g., Sawicki (2012)). Doing this pixel by pixel allows the mapping of star

formation rates (SFR) within galaxies (Sorba and Sawicki, 2015). The history of changes in SFR over time is important for piecing together galactic evolution processes. The improved SED fits will also increase the the accuracy and precision of photometric redshifts. CASTOR is expected to identify a large population of galaxies at high redshift (z=2) (Sorba and Sawicki, 2011). This improvement in redshift accuracy will help link galaxies to large scale structures such as dark halo masses (Darvish, 2016). Therefore CASTOR will help create maps of galactic properties for large scale structures in space and time. This will allow studies of the evolution of galaxies as a function of their environment. The purpose of this work is to simulate how CASTOR will perform for these types of investigations. In particular, how good the observations will be for SED fitting in a variety of galaxies.

Figure 1.2: CASTOR field of view (full image) compared to HST (small square). Consider that surveys done with the HST field of view have yielded 4457 sources for SED fitting. Figure from Côté et al. (2019), used with permission.

1.2.1 PARTNERS

The CASTOR telescope is among several space telescope missions currently in development. It is import to coordinate designs so that observations are complimentary to each other. NASA's Wide-Field Infrared Survey Telescope (WFIRST) is a survey mission in IR bandwidths planned to launch in 2025 (Kruk et al., 2019). WFIRST will expand on HST bandwidths for additional coverage in longer IR wavelengths up to 2μm while also covering a much larger field. ESA's Euclid spacecraft is planned to launch in 2021 (Mellier et al., 2019). It will also cover a large area although in visible and near-IR wavelengths. By cooperating these telescopes will be able to produce large surveys that overlap providing more complete measurements of SED's. This work has incorporated the specifications of WFIRST and Euclid enabling direct comparison with CASTOR.

1.3 MOTIVATION

Whether we want to probe dark matter or the star formation history of galaxies, the telescope has to fit the job. Factors such as the sensitivity of the instrument in different bandwidths, signal to noise ratio and therefore detection limits for specific objects need to be estimated. Simulating images based on proposed telescope designs tests how effective the observations will be. For example we can investigate how much information different exposure times will provide. The simulations will help answer how to perform surveys to get the best data efficiently. The work done here may be useful for an observation planning tool for CASTOR in the future.

Typical exposure simulations estimate the photons gathered for whole objects. For a galaxy this would be based on average surface brightness and SED across the galaxy effectively treating it as a point source (Anderson et al., 2008). This has also been done for CASTOR (Côté, 2018). This does not provide enough information when the structures within the galaxies are the topic of study. What is needed is a pixel by pixel simulation for model galaxies. This allows for exposure calculations of spatially resolved structures within galaxies.

Spatially resolving galactic parameters is important for obtaining accurate overall measurements. For example, it is demonstrated by Sorba and Sawicki (2018) that point source methods underestimate galaxy masses. Using Hubble observations of galaxies in the eXtreme Deep Field (XDF) and pixel-by-pixel SED fitting, Sorba and Sawicki (2018) found that measurements of parameters such as SFR and stellar mass are not accurately represented by average values over a whole galaxy. Figure 1.3 shows the maps generated by this process for SFR and stellar mass. SED fitting is one type of research for which spatially resolve exposure simulations are useful. The model spectra generated by Sorba and Sawicki (2018) for this research are for 4457 galaxies in the XDF. They are used in this thesis as model galaxies to simulating observations form different telescopes. Simulated observations were done for each pixel at previously unobserved wavelengths for all CASTOR, Euclid and WFIRST bandwidths.
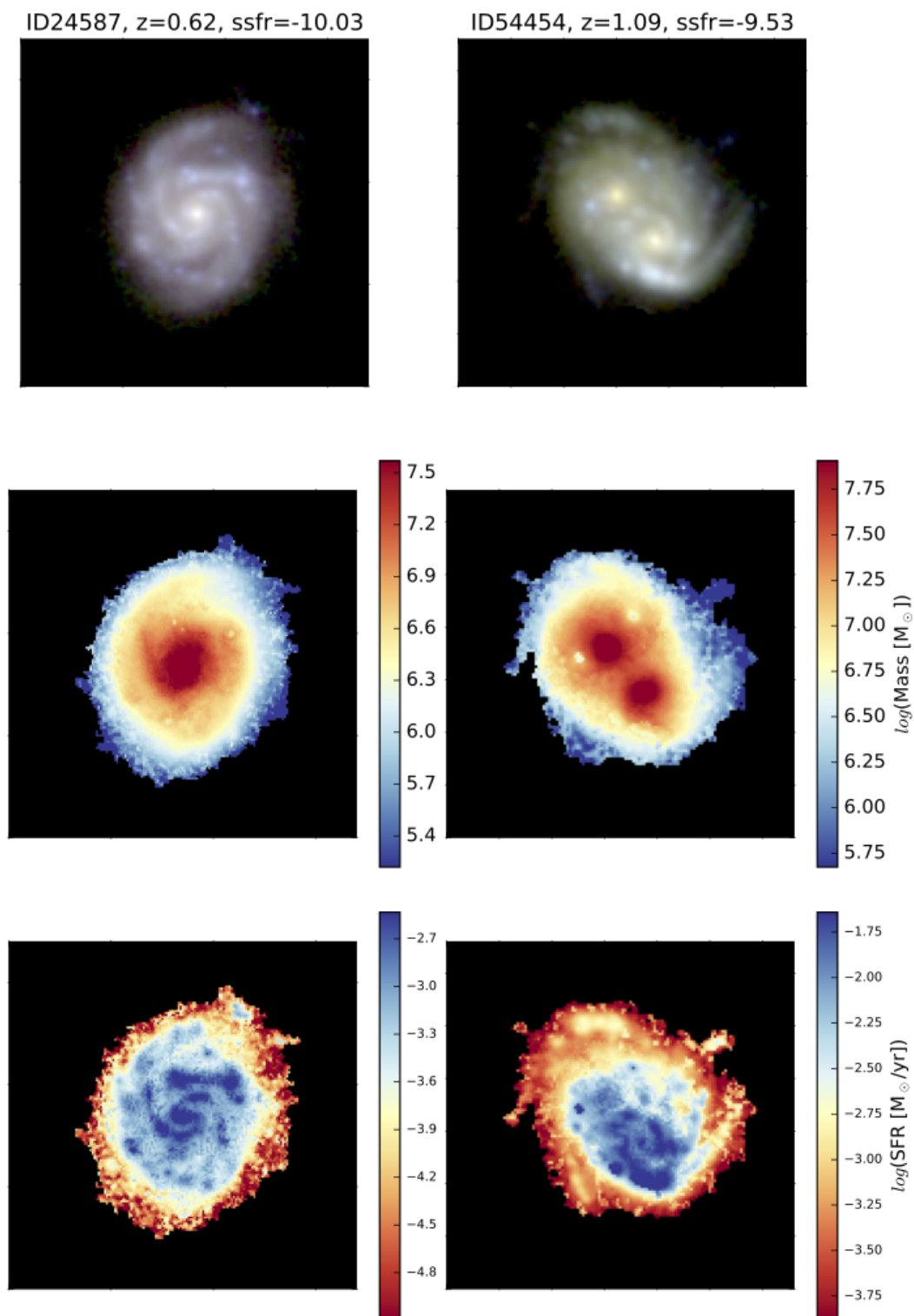
Figure 1.3: Galaxy maps from SED fitting in the HST XDF, top row: visible band colour images, middle row: distribution of stellar mass, bottom row: distribution of SFR. Figure from Sorba and Sawicki (2018), used with permission.

1.4 GOALS

The purpose of this work is to simulate how CASTOR will perform for observations of galaxies where spatial resolution of parameters found through SED fitting such as SFR and stellar mass are important. The simulated images produced allow exposure calculations of spatially resolved structures within galaxies. The simulations can be used to determine optimum exposure times for observations of different objects. This can aid in the planning of more efficient surveys. By incorporating the specifications of WFIRST and Euclid direct comparison with CASTOR is possible. Overlapping surveys can use this information to ensure the observations from different telescopes will work well with each other. The improvement to SED fitting is dependant on a sufficiently complete coverage of galactic spectra.

Chapter 2

Method

2.1 DATA

From Hubble XDF observations Sorba and Sawicki (2018) extracted 4457 extra-galactic sources using watershed segmentation. These Hubble XDF observations consist of images with the magnitudes in several filter bandwidths. The filters, shown in figure 2.1, are f435w, f606w, f775w, f814w and f850lp with the ACS/WFC1 instrument, and f105w, f125w, f140w and f160w with the WFC3/IR instrument. For each pixel in each galaxy Sorba and Sawicki (2018) fit the fluxes in these filters to a galactic spectrum. The spectrum models are spectral energy distributions (SED) modelled using Flexible Stellar Population Synthesis (FSPS) (Conroy et al., 2009). This method is called SED fitting and an example fit is shown in figure 2.1. For the FSPS models solar metallicity, Chabrier (2003) initial mass function, Calzetti (2000) dust law and Byler (2016) nebular line emission were assumed. The models were corrected for extinction due to intergalactic hydrogen (Madau, 1995). Fit parameters included mass, star formation history (exponential decay) and dust. More information about the assumptions and fit parameters are outlined in the paper (Sorba and Sawicki, 2018). Of the 9 bands fit, the F160W had the lowest spatial resolution with a FWHM of 0.2 arcseconds. The rest of the images were convolved to match this
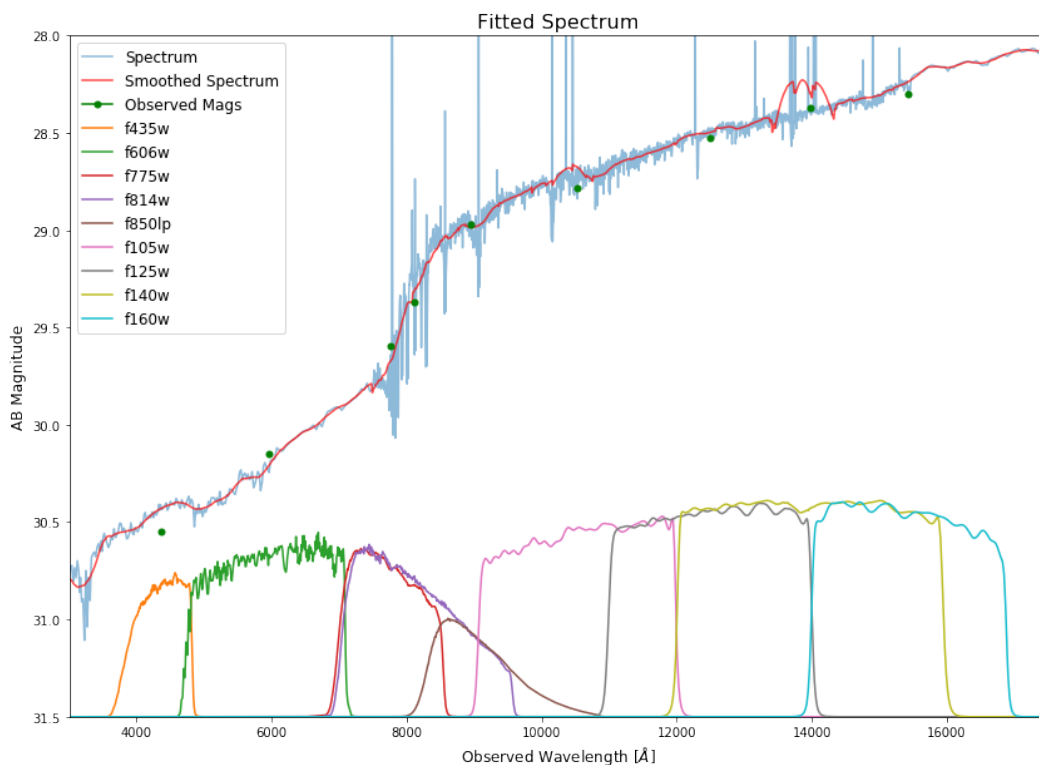
Figure 2.1: Observed Hubble magnitudes (green dots) with a fitted FSPS spectrum for one pixel in example galaxy 24587 (z=0.62, F140W AB=19.6). Below the spectrum the response curves of the 9 Hubble filters are plotted.)

resolution during the spectra fitting process (Sorba and Sawicki, 2018). This is the upper limit of resolution for images produced by the methods outlined below.

What is important for this work is there is now a catalogue from which the galactic spectra for each pixel can be loaded. The pixels can be sorted by various parameters including Rafelski ID number, Redshift and Magnitude.The Rafelski ID refers to the spectroscopic and photometric redshift catalog from Rafelski (2015) which also contains AB magnitudes in Hubble filters. The distributions of these sources in redshift and magnitude is shown in figure 2.2. Spectroscopic redshifts are used where available otherwise photometric redshifts are used. A selection was made from this distribution shown in red in the figure. This selection brackets a representative sensitivity range
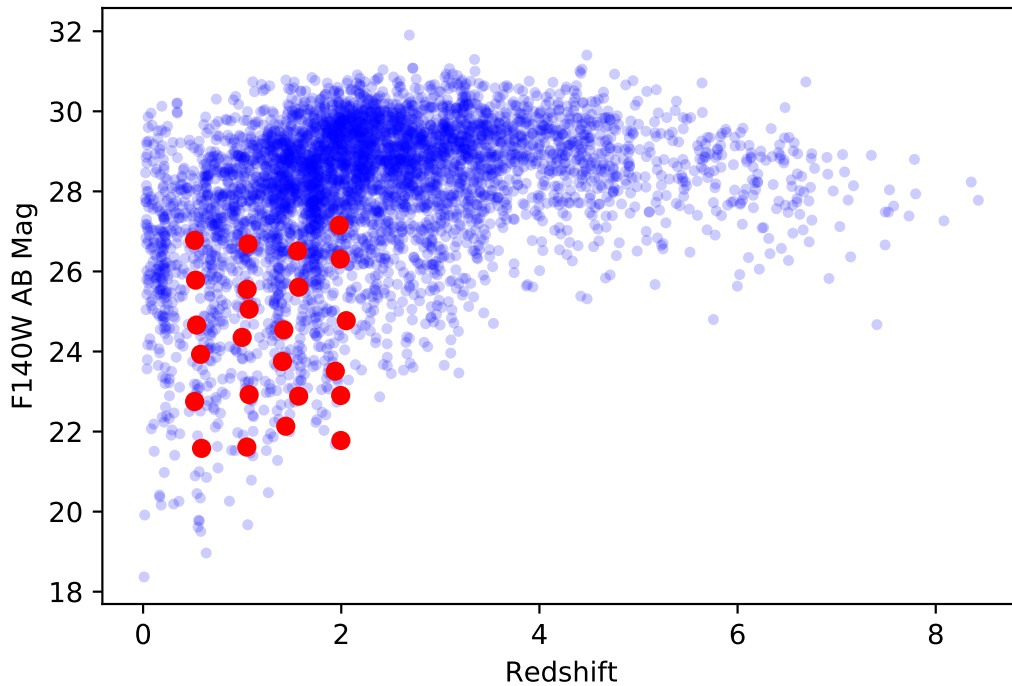
Figure 2.2: Distribution in redshift and magnitude of 4457 processed galaxies. Red dots show a selection galaxies used for discussion of the results in chapter 4.

for CASTOR that is used for further analysis in chapter 4.

2.2 SIMULATION

2.2.1 IMAGES

To simulate an image of a galaxy from spectra in the catalogue the appropriate pixels and spectra were first assembled based on the galaxy ID number. Then the spectra are processed to give the flux observed by the telescope and this depends on the response curve of the telescope. The technical specifications of the telescopes optics and sensor can be represented as a spectral response curve. A response curve combines wavelength dependant information about the telescope such as mirror and

detector efficiencies into one transmission curve. The response curves can be updated

as decisions are made about the telescope design.

Convolving a galactic spectrum with the response curve gives the spectrum avail-

able for observation by the telescope. From the observed spectrum the photon count

can be determined for a given exposure time but before that the accuracy of this

method should be addressed. The AB magnitude can also be modelled from this

observed spectrum. Using Equations 2.1 and 2.2 from Sawicki (2012) the magnitudes

were modelled for each of the original Hubble filters and their response curves. In

Equation 2.1 $T_i(\lambda)$ is the transmission for a filter i. The galactic spectrum ($f_\nu(\lambda)$) in

units of $ergs/s/cm^2/hz$ is combined with the transmission and wavelength (λ) to give

the modelled flux in filter i. The modelled flux (f_ν, i) also in units of $ergs/s/cm^2/hz$

is then converted to AB magnitude using Equation 2.2.

$$f_{\nu,i} = \frac{\int f_\nu(\lambda)\lambda T_i(\lambda)d\lambda}{\int \lambda T_i(\lambda)d\lambda} \tag{2.1}$$

$$m_{AB} = -2.5\log f_{\nu,i} - 48.60 \tag{2.2}$$

These modelled magnitudes were compared with the original magnitudes from

the Hubble images to check for consistency. Figure 2.3 shows how these magnitudes

compare for a pixel in galaxy 24578. The modelled magnitudes differ from the origi-

nals by about 0.1 mag in the example figure and similarly for other pixels and other

galaxies. This uncertainty is acceptable for the exposure simulation since the main

purpose of this method is to have a distribution of realistic galaxies not necessarily
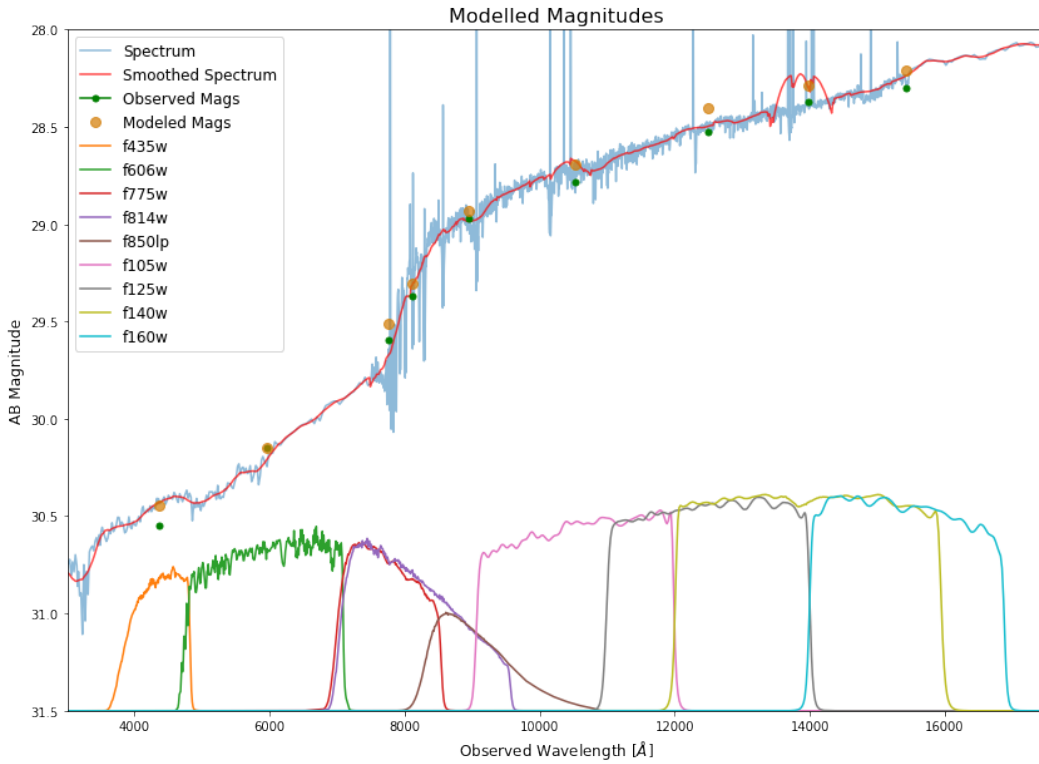
Figure 2.3: Modelled Hubble filter AB magnitudes show agreement with the fitted spectrum and observed magnitudes. Below the spectrum the response curves of the 9 Hubble filters are plotted. For Galaxy 24578 with z=0.62 and F140W AB=19.6.

the exact galaxies.

To simulate the photons counted during an exposure the observed flux is integrated over the filter response. This is shown in Equation 2.3 where $F_p h(\lambda)$ is the source spectrum in units of $photons/s/cm^2/\mathring{A}$. The resulting photon rate in a filter, $F_{ph,i}$, is left in units of $photons/s/cm^2$ to allow for modelling of different telescopes later on. By later applying the aperture of the telescope and gain of the detector electron counts are produced for a given exposure length. By doing this for each pixel an image array is generated in a given filter. Figure 2.4 shows the Hubble (listed in 2.1), CASTOR, WFIRST and Euclid filters for which this processing was done.

$$F_{ph,i} = \int F_{ph}(\lambda)T_i(\lambda)d\lambda \qquad (2.3)$$

The CASTOR filters processed include: 400-550 nm (G), 300-400 nm (U), 260-400 nm (wide U), 150-300 nm (UV) and 135-260 nm (short UV). These are provisional because the whole optical system, including the detector QE, is being modelled at JPL and will change (Côté, 2018). The response files were created by Côté (2018) using the detector quantum efficiency (DQE) for the CIS113 detector and some reasonable assumptions about coatings and dichroics.

The WFIRST filters processed include: F184, J129, Y106, G150, R062, Z087, H158 and W146. The filters are from The Spanish Virtual Observatory's (SVO) Filter Profile Service (Rodrigo et al., 2019). Since SVO did not include the DQE the efficiency of the Teledyne H2RG (2.5 micron cutoff) detector was added to the filter profiles to make the response curves used. WFIRST plans to use H4RG-10 which has a different pixel size, but QE will not change much (Iwata, 2018).

The Euclid (NISP0) filters processed include: Blue,J,Y,H and Red. The response curves are from SVO Filter Profile Service and did include DQE (Rodrigo et al., 2019).

To process the 4457 galaxies in the XDF catalogue the ACENET Graham computing cluster was used. Using information learned from ACENET tutorials and meeting with ACENET support, the code was redeployed into an optimized package that ran the galaxies in batches on the cluster. Figure 2.5 shows a new XDF field with image data simulated for the CASTOR short UV filter response. The output
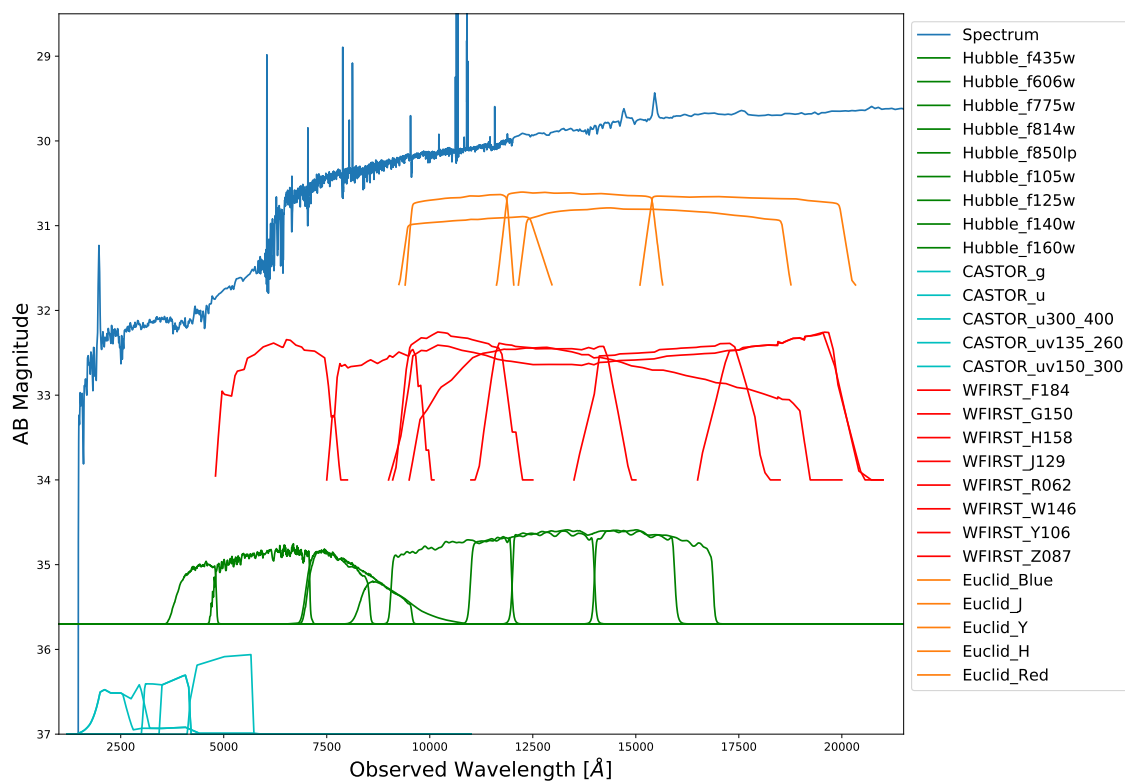
Figure 2.4: The CASTOR (Cyan), Hubble (Green), WFIRST (Red) and Euclid (Orange) filter responses for which images were processed. Plotted spectrum is for a pixel in galaxy 24578 with z=0.62 and F140W AB=19.6
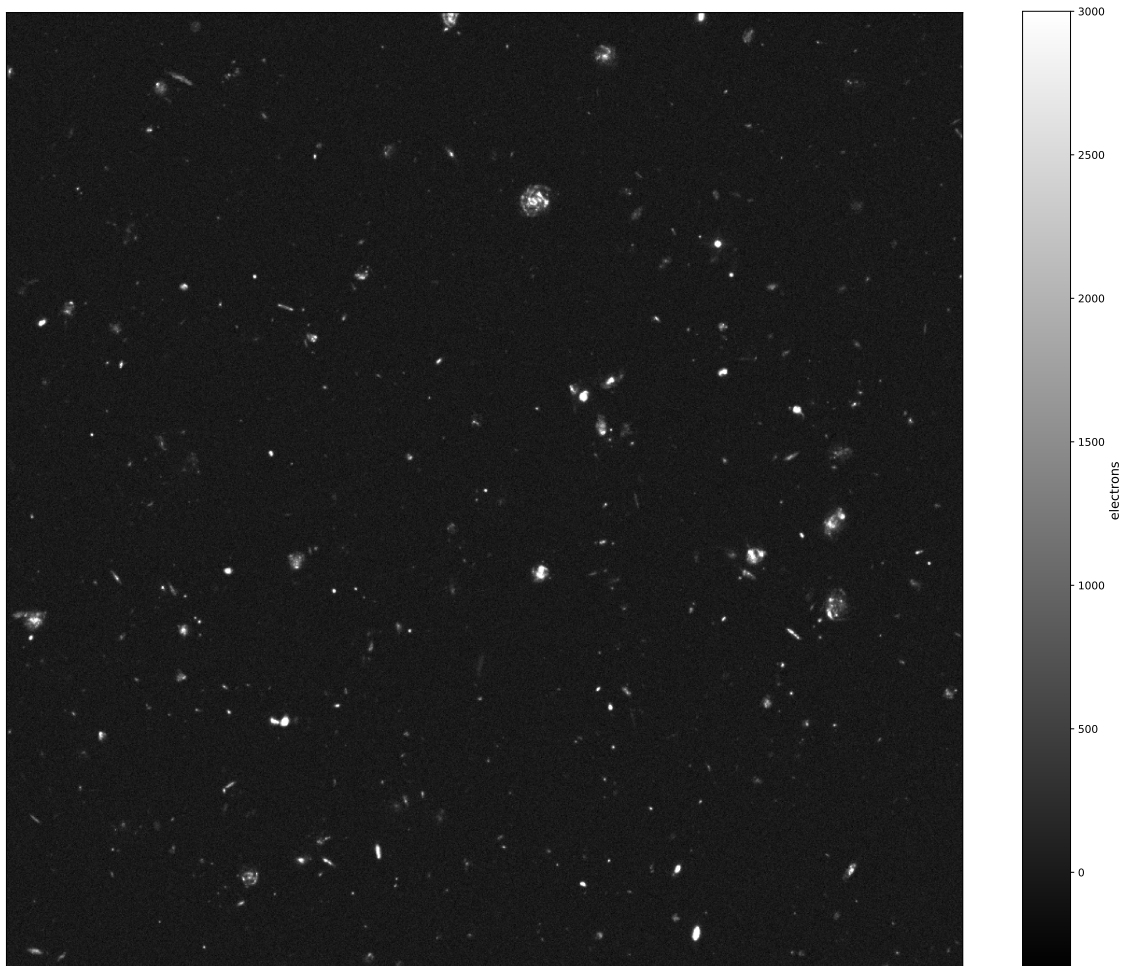
Figure 2.5: Simulated XDF Field in CASTOR Short UV filter with resampling and noise (described in following sections) for a 100 hour observation. FITS files of XDF images for all CASTOR filters are included with this thesis.

of the image simulation is in units of $photons/s/cm^2$ and represents only the signal from a galactic source. Post processing is required to create the final image. For the example in Figure 2.5 exposure time, aperture, pixel scale and gain for CASTOR has been applied. The noise for an 100 hour observation has also been simulated. The post processing and noise simulation are described in the following sections.

2.2.2 RESAMPLING

The original Hubble images after dithering have a pixel scale of 0.06 arcseconds (Sorba and Sawicki, 2018). The geometry of the focal plane for CASTOR may still change. This simulation assumes a 2x8 layout with pixels in 1920x5760 array covering 0.383 deg x 0.512 deg of sky. This translates to a pixel scale of 0.12 arcseconds. A supplementary program was written to resample the image to a new image scaled by a constant factor to the nearest integer number of pixels in height and width. The constant factor is the Hubble pixel scale divided by the new telescopes pixel scale. So for CASTOR the factor is 0.5 and the new image is half the pixels in height and width. To preserve flux the fluxes in each pixel from both images are summed and the new images total flux is scaled to match the total flux in the image with the original Hubble sized pixels. This was also done for WFIRST which has a pixel scale of 0.11 arcseconds.

The original resolution (FWHM) of the Hubble images is 0.20 arcseconds (see Section 2.1). The broadest resolution (which is the limiting value for SED fitting) for CASTOR is 0.17 arcseconds in the g filter. WFIRST will produce images with a resolution of comparable to Hubble as it will have the same aperture of 2.4 meters (Kruk et al., 2019). The broadest filter is reported to be 0.14 arcseconds (Spergel et al., 2013). It was decided to not artificially sharpen the the Hubble images and introduce artifacts. The approximate resolution is sufficient for the purpose of exposure simulation and for a given example galaxy it could be factored in that a slightly smaller galaxy then the original is being observed.

2.3 NOISE

An image is comprised of counts generated from source photons as well as noise from various sources. The noise accumulated in an observation is determined from background radiation and sensor specifications. Background radiation is counted during an exposure, however in practice the median of these counts is removed using background subtraction methods. This still leaves the noise present in the background counts and that is what needs to be simulated. On the sensor noise is contributed from readout of the pixels and from dark current. Dark current is subtracted similarly to background. For background and dark current subtracted images the noise is simulated from the expected standard deviation for a given count from these sources. For a photon counting detector the standard deviation is the square root of counts from a given source. Factoring in gain, which for CASTOR is 2.0 photons/electron, gives a final value in units of electrons for noise counted by the sensor. Equation 2.4 shows how sources of noise are combined to give a signal to noise ratio (SNR) in a pixel of image data (Fellers and Davidson, 2019).

$$ SNR = \frac{Pat/g}{\sqrt{(P + B\rho^2)at/g + Dt + \sigma_R^2}} \tag{2.4} $$

In the equation P is the source rate. This rate is from Equation 2.3 and therefore in units of $photons/s/cm^2$. The background rate B is in units of $photons/s/cm^2/arcsec^2$. The aperture area of a given telescope is a where $a = \pi(D/2)^2$ for diameter D. The diameter of CASTOR is planned to be one meter (Côté et al., 2012). For WFIRST the diameter is 1.5 meters (Côté et al., 2012). The area of the sky that a given pixel

observes is the pixel scale ρ squared. The pixel read noise is σ_R (2.9 electrons for CASTOR (Côté, 2018)), and D is the dark current rate (0.01 electrons/s for CASTOR (Côté, 2018)). The exposure time for an observation is t. The noise scales with the square root of the exposure time. The read noise is a constant deviation per pixel and exposure. While the source signal scales linearly with exposure time.

So far this gives the standard deviation of the noise. To simulate a realistic image each pixel receives a random value from a Gaussian distribution. The mean of the Gaussian the modelled source counts and standard deviation is found from Equation 2.4. An example of the code written to find the noise from various sources and simulated an image is included in Appendix C.

2.3.1 CASTOR NOISE

To simulate noise for CASTOR, first all potential sources for background radiation were estimated. The background sources include terrestrial, solar system, galactic, and extra-galactic sources. In Earth orbit sources of noise affecting CASTOR bandwidths include Earthshine and the 2471 angstrom O II geo-coronal emission line (Anderson et al., 2008). Earthshine consists of solar radiation reflected by earth and residual air glow (Giavalisco et al., 2002). This depends on the angle between the telescope pointing and the limb of the Earth (Limb Angle). For this project a spectrum was used for a high noise case of 38 deg. The values adopted are shown in Table 2.1. The high noise case represents the upper limit of observations that would actually be performed.

Zodiacal light is a source of background from solar radiation reflected by inner solar system dust (Giavalisco et al., 2002). Zodiacal light depends on ecliptic latitude and longitude and the spectrum for a high noise case was used for 30 and 45 degrees respectively (Giavalisco et al., 2002). A "local" background spectrum was created using combined zodiacal light and Earthshine spectrums with the geo-coronal line added. The background spectrum was processed similarly to the galactic spectrum in Section 2.2.1 to get the photon count rate in a given filter. This local background spectrum is shown in Figure 2.6 with CASTOR filters overlaid for reference. This gives close agreement to values obtained with the Hubble exposure time calculator (ETC). The Hubble ETC was used to simulate the background in a pixel using Hubble response files. These values where compared to the method used here for the same response files and exposure time, as well as compensating for aperture and gain differences. The agreement is within one percent.

The Galactic source of background in the UV is a diffuse flux vastly dominated by starlight scattered by interstellar dust (Bowyer, 1991). The flux of the background varies with galactic latitude as shown in data from GALEX (Murthy, 2014). A high value ($1000\ ph\,cm^{-2}s^{-1}sr^{-1}\mathring{A}^{-1}$ (Murthy, 2014)) was used corresponding to approximately 40 deg north galactic latitude.

Some extragalactic flux (approximately $100\ ph\,cm^{-2}s^{-1}sr^{-1}\mathring{A}^{-1}$) is present in the UV and mainly consists of redshifted starlight from unresolved galaxies (Bowyer, 1991). The combined values of galactic and extragalactic background were used as a constant function and convolved with the CASTOR filter bandpasses to give an estimated non-local background flux. This value is based on the FUV bandwidth and
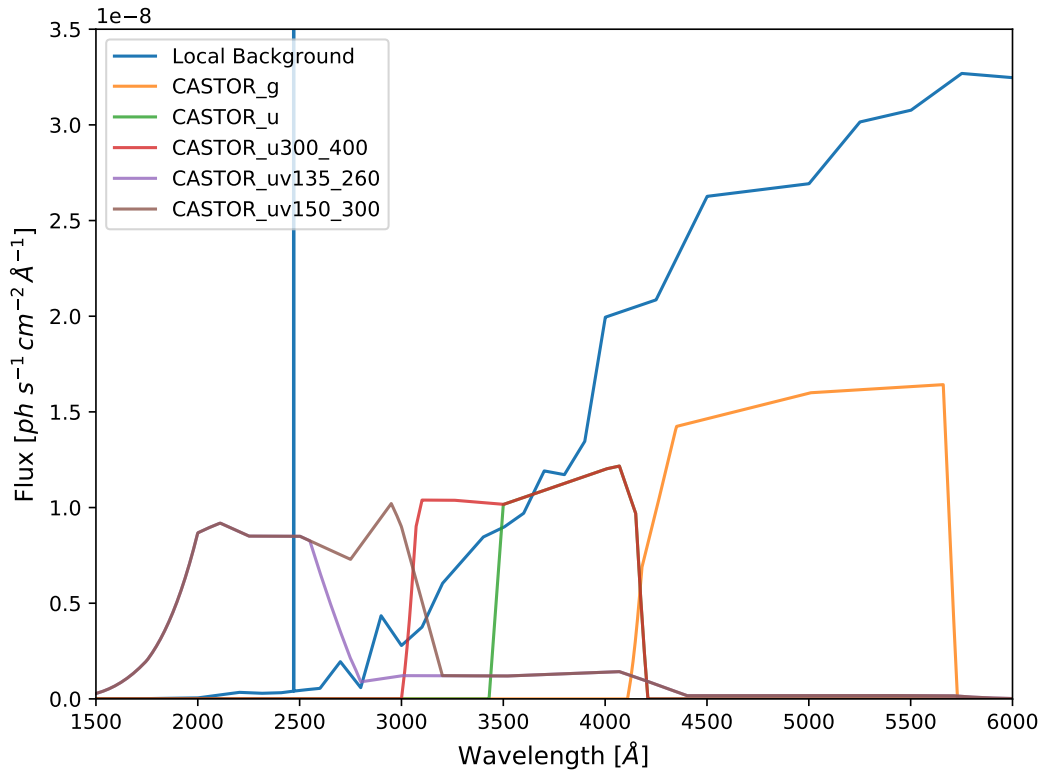
Figure 2.6: Local background spectrum with filter responses for CASTOR.

Table 2.1: Noise Contributions for the CASTOR Short UV filter

Source	Intensity $(ph\,cm^{-2}s^{-1}sr^{-1}\mathring{A}^{-1})$
Zodiacal Light and Earthshine	14703
Geocoronal	100
Galactic	1000
Extra-Galactic	100

becomes a worse approximation in the visible band, although this is not significant as local background sources heavily dominate there. In fact, it is necessary to observe in the FUV to accurately measure these values (Bowyer, 1991). Table 2.1 shows flux values from all sources for comparison. Even in the Castor Short UV filter the local sources of background are far more significant.

Having compiled all sources of noise for CASTOR the XDF field can be simulated with noise and resampling as shown in Figure 2.5. Another useful way to visualize
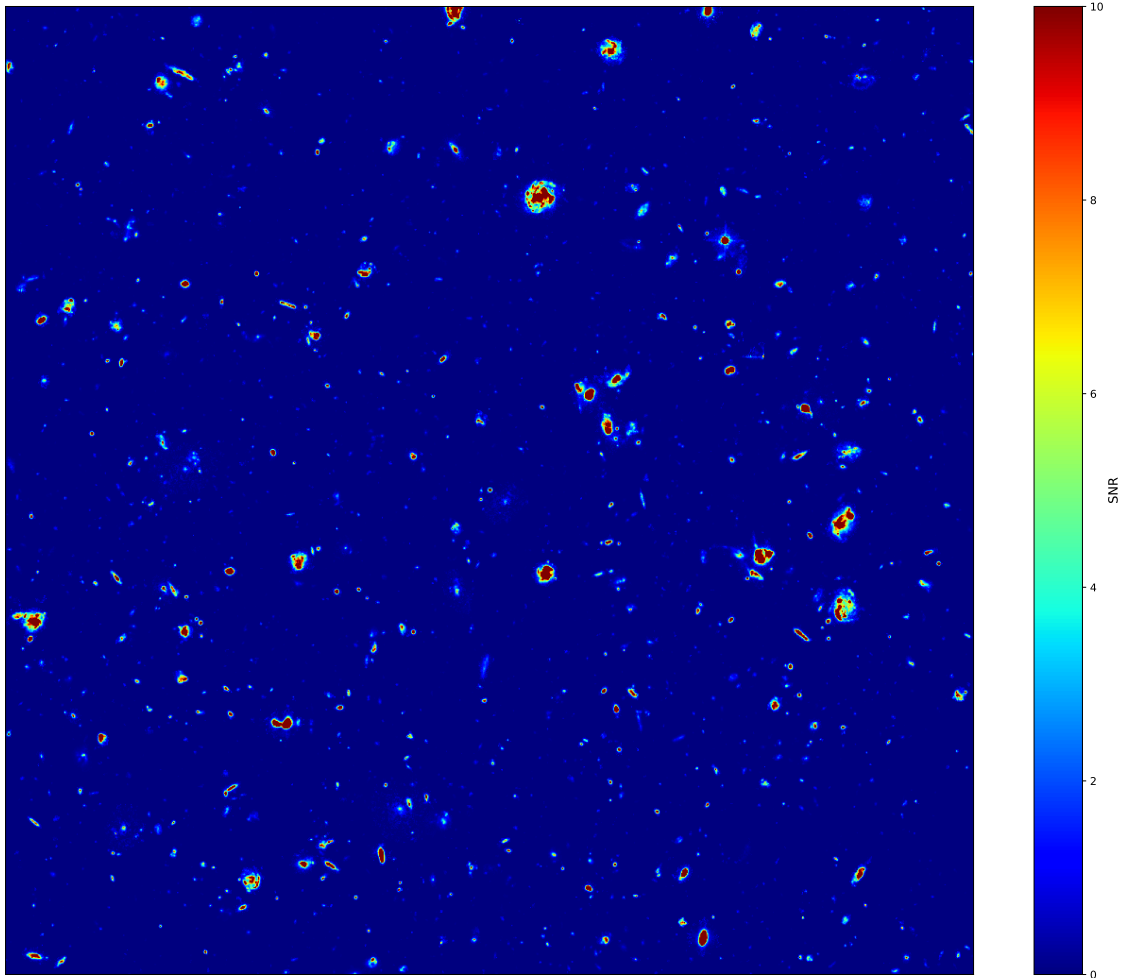
Figure 2.7: Simulated SNR map of the XDF Field in the CASTOR Short UV filter for a 100 hour observation. The colour scale is normalized from 0 to 10 SNR. FITS files of XDF SNR maps for all CASTOR filters are included with this thesis.

these results is with a map of the SNR found from Equation 2.4. Figure 2.5 shows an SNR map for the XDF field in the CASTOR Short UV filter for a 100 hour observation.

2.3.2   Low Noise Case

The high noise cases outlined above are not extreme but rather the upper limit that would be found in real observations. Provided here is an estimate of a low noise

case given the best conditions. Assuming the detector specifications remain constant all that is need is to estimate the change in background and see how that change affects the overall SNR. In Table 2.1 it is shown that the local background, namely zodiacal light and Earthshine are the dominant sources of noise. For increasing Limb Angle the Earthshine drops of rapidly so for a low noise case it can be assumed that zodiacal light is dominant (Anderson et al., 2008). The flux from zodical light for the lowest case of 90 and 180 degrees (ecliptic latitude and longitude) is approximately 30 percent of the high case (Anderson et al., 2008). For a 100 hour exposure this translate to an 8 percent increase of the SNR in the CASTOR short UV filter. Up to a 20 percent increase in the SNR is expected in the wide U filter for a low noise case. The wide U filter is the filter most affected by local noise, this is discussed in Section 4. Comparing high and low cases for galactic noise from galactic latitudes ranging from 30 to 90deg results in less than 0.5 percent increase in SNR for all filters.

2.3.3 WFIRST Noise

The noise for WFIRST was also derived for comparison to the CASTOR results. For WFIRST an analysis of the noise similar to the above for CASTOR is already available and using results from that the noise for an image simulation was reconstructed. In Kruk et al. (2019) the sensitivity in each filter is given as the limiting AB magnitude for a 5 sigma detection with a one hour exposure. The sensitivities were converted to a total variance rate in electrons/second for each filter. This was combined with the simulations of the galaxy images for WFIRST response curves at given exposure
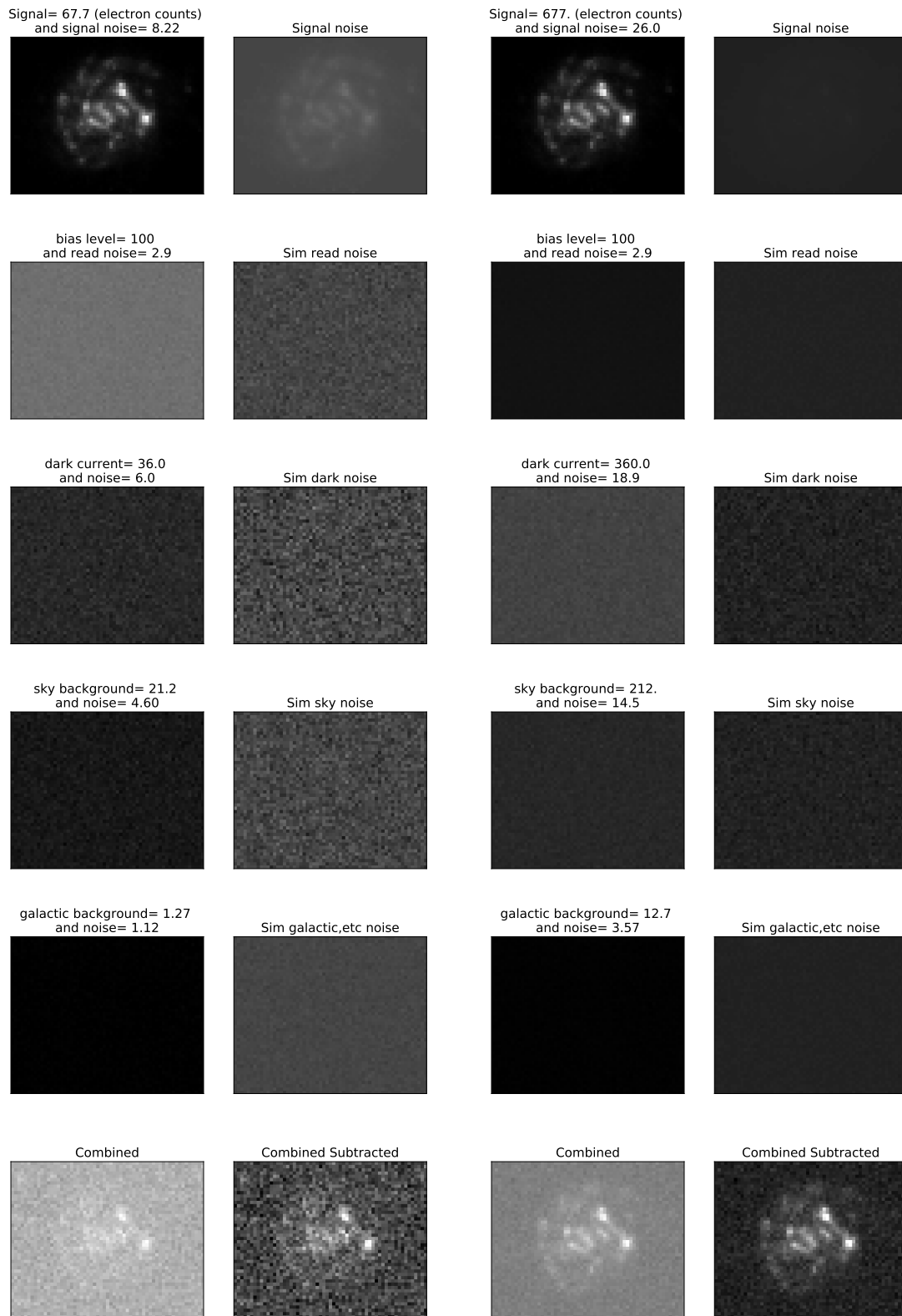
times.

Chapter 3

Results

3.1 BREAKDOWN OF IMAGE LAYERS

To examine the results more closely this sections focuses on an example galaxy (Rafelski ID: 24587, z=0.62, F140W AB=19.6). Figure 3.1a shows the layers that make up a simulated image. Each layer corresponds to the sources of signal or noise outlined above. The left column shows the counts from the contributing source as well as the noise in those counts. The right column shows only the resulting noise. For example, the fourth row shows the local "sky" background counts and noise on the left and only the noise as if for a background subtracted image on the right. Each image in a column shares the same normalization from the highest and lowest values of the last row of images. The last row is an exception where all the layers are combined according to Equation 2.4 with the source signal to show the final product. Figure 3.1b shows the effect of increasing the exposure time from 1 hour to 10 hours on each layer.

Signal= 67.7 (electron counts) and signal noise= 8.22

Signal noise

Signal= 677. (electron counts) and signal noise= 26.0

Signal noise

bias level= 100 and read noise= 2.9

Sim read noise

bias level= 100 and read noise= 2.9

Sim read noise

dark current= 36.0 and noise= 6.0

Sim dark noise

dark current= 360.0 and noise= 18.9

Sim dark noise

sky background= 21.2 and noise= 4.60

Sim sky noise

sky background= 212. and noise= 14.5

Sim sky noise

galactic background= 1.27 and noise= 1.12

Sim galactic,etc noise

galactic background= 12.7 and noise= 3.57

Sim galactic,etc noise

Combined

Combined Subtracted

Combined

Combined Subtracted

(a) For a 1 hour observation.

(b) For a 10 hour observation

Figure 3.1: Noise simulation layers for Galaxy 24587 (z=0.62, F140W AB=19.6) in the CASTOR Short UV filter for 1 and 10 hour observations.

3.2 COMPARING FILTERS

This section summarizes the final images in all the bandpasses that images and noise were simulated. This includes all CASTOR and WFIRST filters (there was not enough time to prepare a treatment of noise for Euclid). Figures 3.2 and 3.3) show the final images for the example galaxy at several exposure times. From these figures it can be seen that some filters perform better than others at a given exposure. Also the WFIRST simulation have produced much cleaner images when compared to CASTOR at identicle exposure times. This is expected given the larger aperture of WFIRST.

Figures 3.4 and 3.5) show the SNR maps for each filter. The colour scale in these figures is normalized from 0 to 10 SNR. The max cut off for the colour was chosen at 10 as that is generally considered more than enough for most observations. It can be seen from these figures that WFIRST can reach 10 SNR in much less exposure time than CASTOR. Also since the final three filters for CASTOR are not yet finalized these figures could be aid the decision. The choices are between the 300-400 nm (U) or 260-400 nm (wide U) filters and the 150-300 nm (UV) or 135-260 nm (short UV) filters. If only the best SNR for a given exposure time is considered, then Figure 3.4 suggest that the U (300-400 nm) and UV (150-300) are the optimal filters. The wide U and short UV produce less regions at 10 SNR for the same exposure time.

The differences in noise amongst the CASTOR filters can generally be explained by two opposing factors. The contribution from the local background noise increases from short to longer wavelengths as can be seen in Figure 2.6. In Section 2.3.1, it
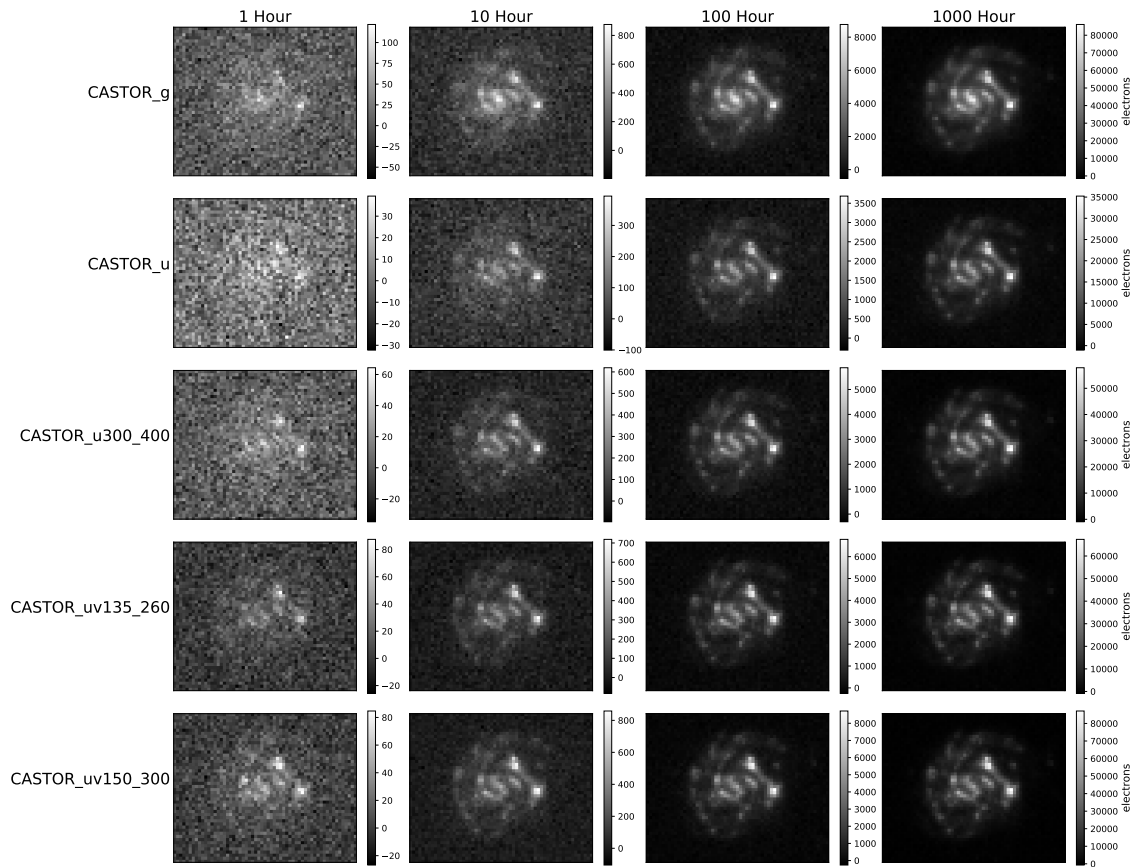
Figure 3.2: Galaxy 24587 image processed in all CASTOR filters for exposure times of 1,10,100, and 1000 hours.

was found that when present the local sources of noise dominate over galactic and extra-galactic sources. The signal from a typical galactic spectrum also increases from short to longer wavelengths as can be seen in Figure 2.4. These competing trends between signal and noise results in the apparent turn over in the wide U bandwidth making it the band most affected by noise.
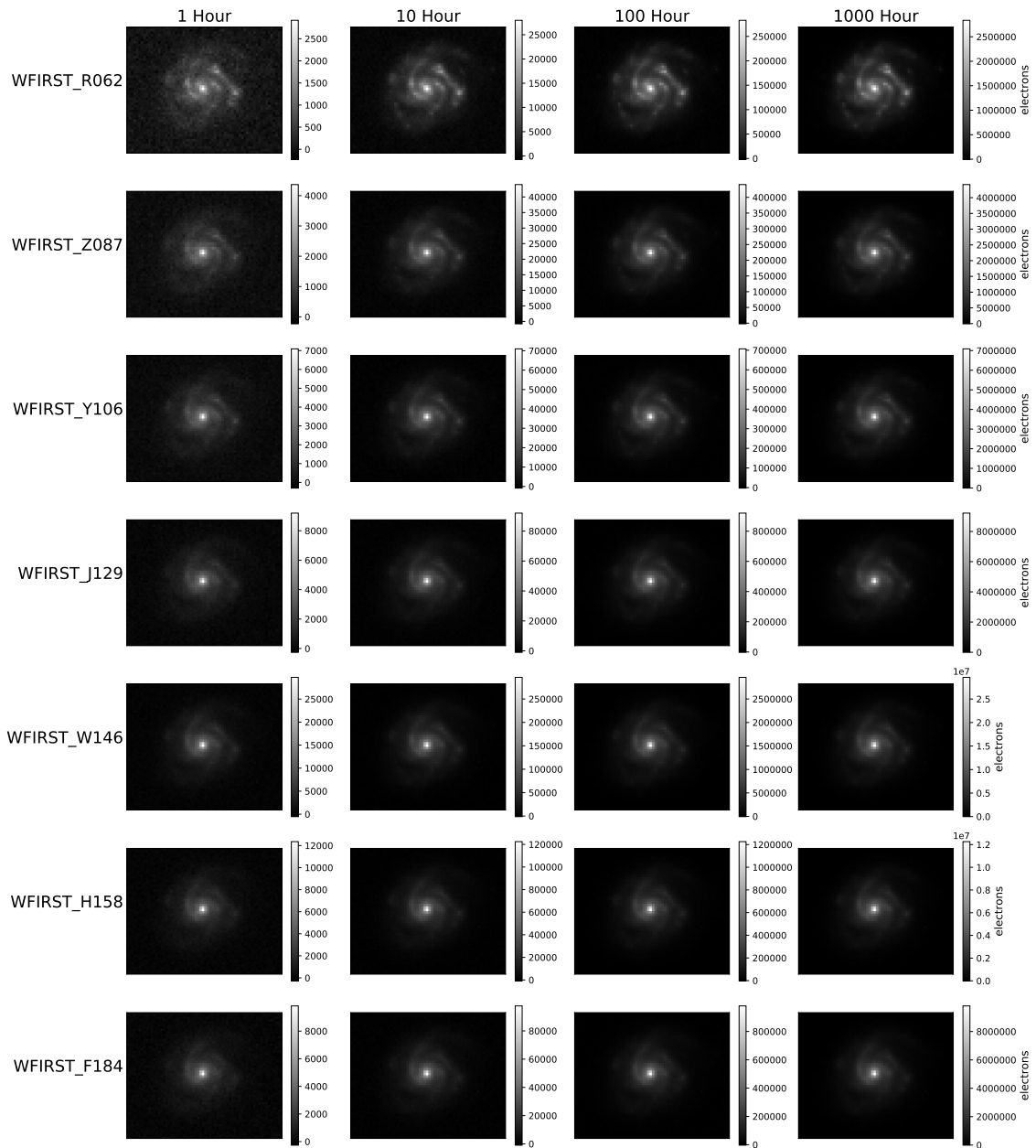
Figure 3.3: Galaxy 24587 image processed in all WFIRST filters for exposure times of 1,10,100, and 1000 hours.
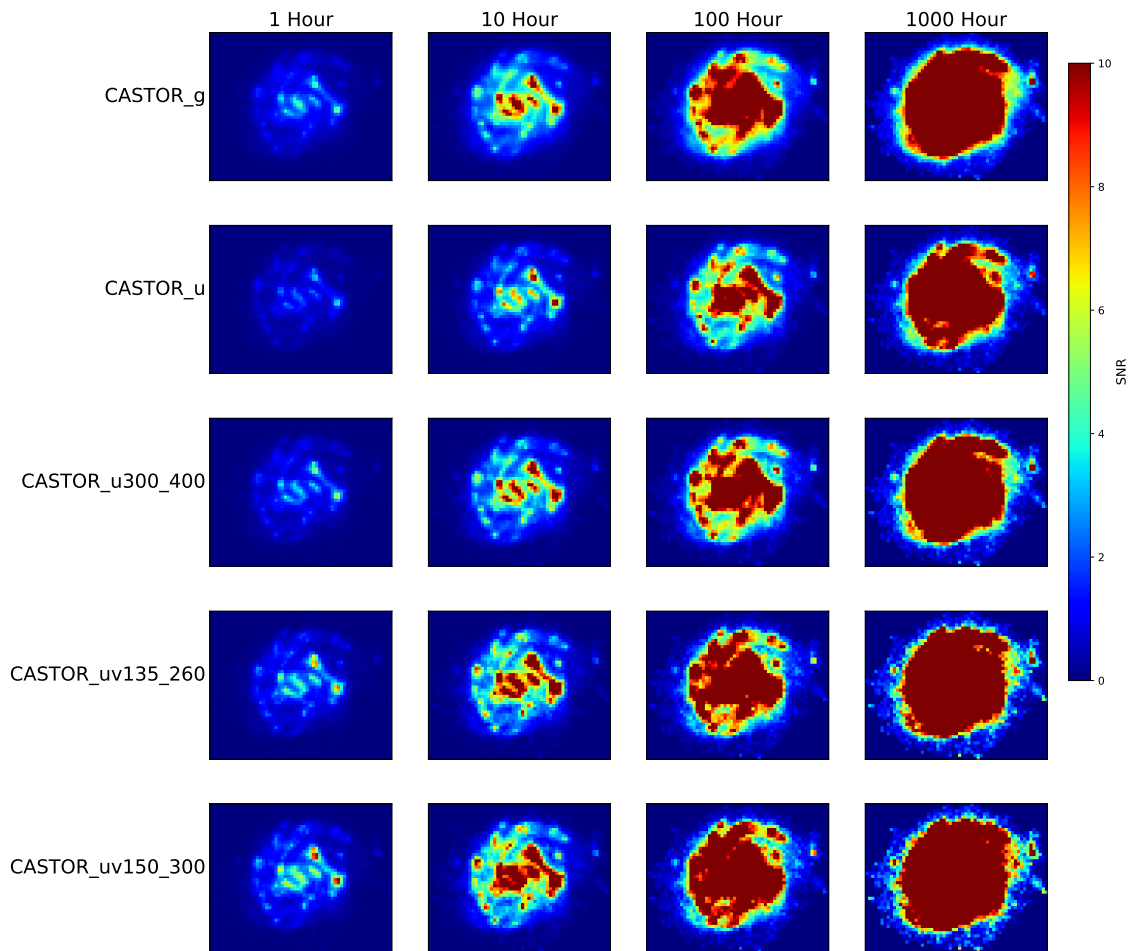
Figure 3.4: Galaxy 24587 SNR map processed in all CASTOR filters for exposure times of 1,10,100, and 1000 hours. The colour scale in these figures is normalized from 0 to 10 SNR.
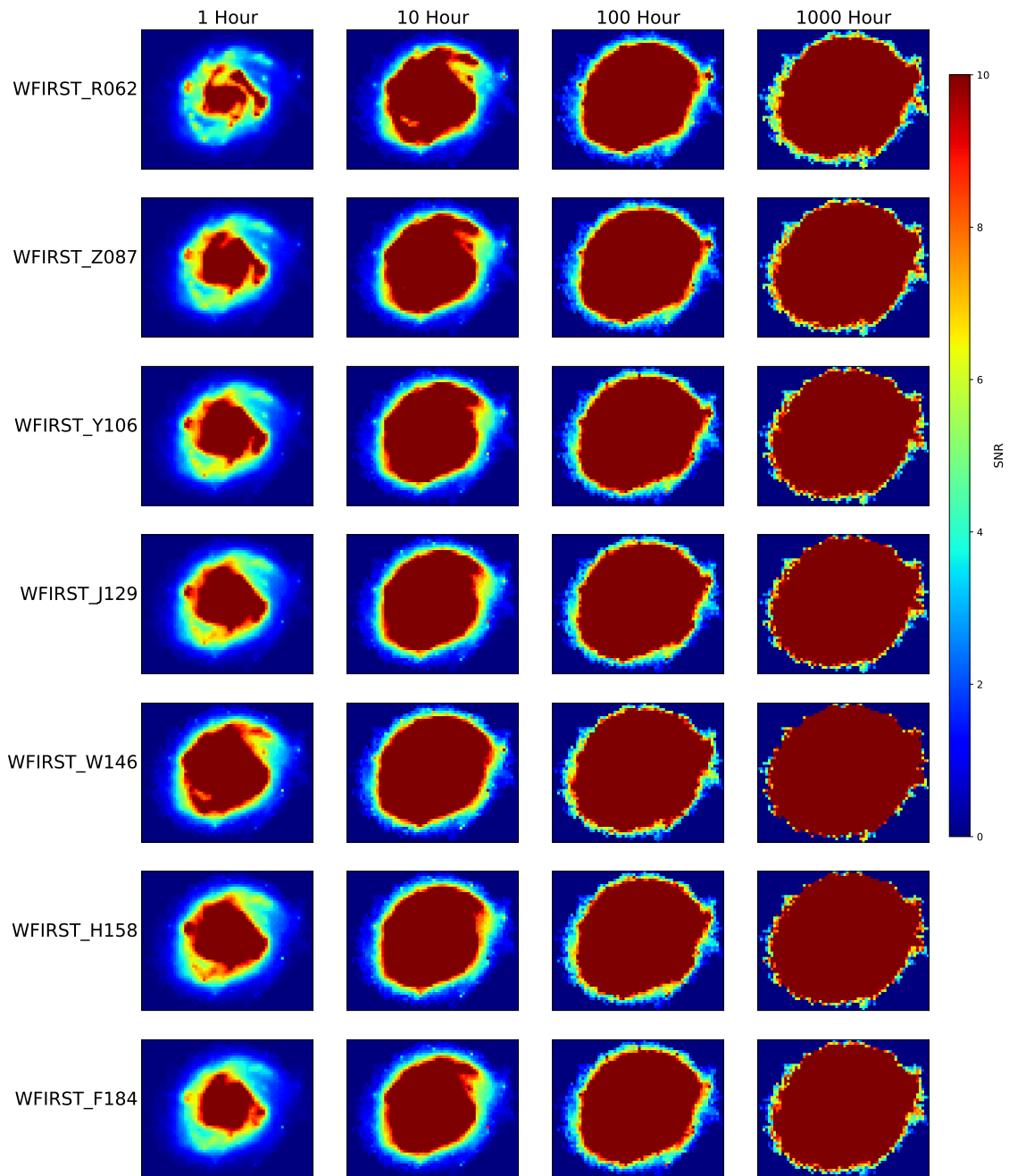
Figure 3.5: Galaxy 24587 SNR map processed in all WFIRST filters for exposure times of 1,10,100, and 1000 hours. The colour scale in these figures is normalized from 0 to 10 SNR.

3.3 RGB IMAGE EXAMPLE

False colour images are used to visualize image data from different filters. Three observation of different bandpasses are assigned to RGB channels to create a colour image. An example is shown in Figure 3.6 without resampling and noise and in Figure 3.7 with resampling and noise. In each image green represents the CASTOR G filter, blue represents the CASTOR Short UV filter and red represents the WFIRST F184 filter. The challenge of doing this is more artistic then scientific since the photon counts vary for different bandwidths and especially for different telescopes. The normalization for each channel was set in an attempt to not favour any of the three since a neutral combination makes the differences between the channels become more apparent.
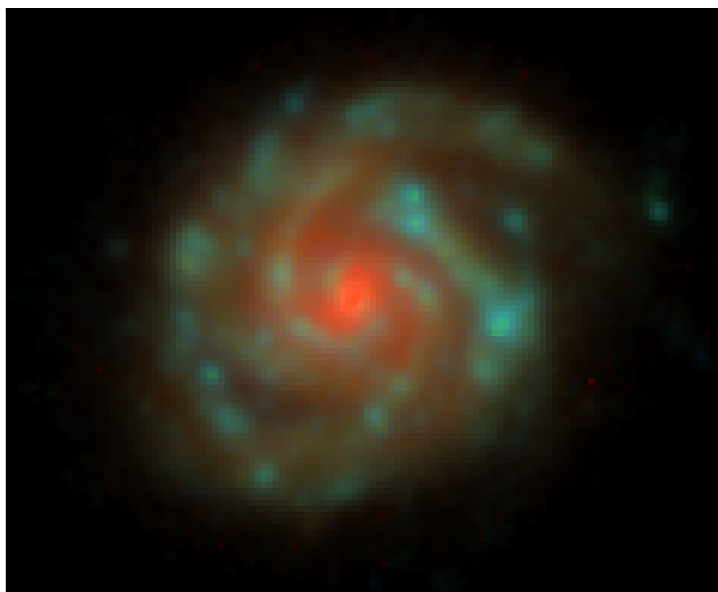
Figure 3.6: False colour image of galaxy 24587 in CASTOR G, FUV and WFIRST F184 filters. Green represents the CASTOR G filter, blue represents the CASTOR Short UV filter and red represents the WFIRST F184 filter.
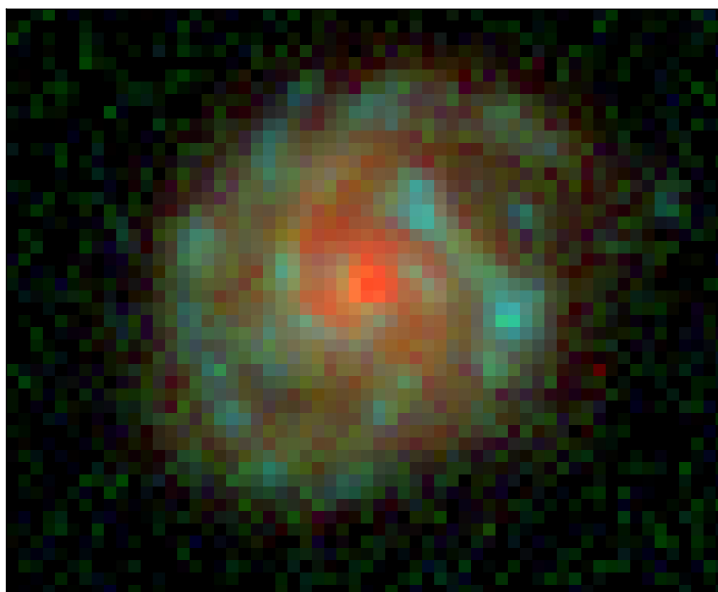

Figure 3.7: False colour image of galaxy 24587 in CASTOR G, FUV and WFIRST F184 filters. With resampling and noise for an exposure time of 100 hours. Green represents the CASTOR G filter, blue represents the CASTOR Short UV filter and red represents the WFIRST F184 filter.

Chapter 4

Discusion

4.1 Comparing Magnitudes and Redshifts

Figure 2.2 in Section 2.1 shows the distribution of the 4457 galaxies processed plotted with respect to their magnitude and redshift. Of these galaxies a selection was made of galaxies on a grid with redshifts (0.5,1.0,1.5 and 2.0) and AB magnitudes (22,23,24,25,26 and 27 in the Hubble F140W filter). The images and SNR maps for this selection grid of galaxies were plotted for all CASTOR and WFIRST filters. For CASTOR 100 hour observations were simulated. For WFIRST shorter 10 hour observations were simulated, which corresponds to a typical observation with the telescope given the better sensitivity. The galaxies images were padded to a constant field of view with an area of $24\,arcsec^2$. These images are included in Appendix A.

Derived from the grids of SNR maps, the pixel by pixel minimum SNR of the filters was used to create a new grid of SNR maps. For WFIRST each pixel in Figure 4.2 represents the minimum SNR value of all the WFIRST filters. For CASTOR each pixel in Figure 4.1 represents the minimum SNR value of three select filters. The filters selected are the G U and UV filters as the wide U and short UV filters were found to be less efficient in Section 3.2. An SNR of 5 is generally adopted as a requirement for SED fitting methods (Sorba and Sawicki, 2018). So for such research

the figures show objects that (for the exposure times) range from easy to observe (for low redshift and brighter magnitudes) to difficult to observe (for high redshift and fainter magnitudes).

4.2 The Differences Between GALEX and CASTOR Filters

The noise analysis for CASTOR done in this work shows that the UV filter options are sensitive to large contributions from the local background spectrum consisting of Zodiacal light and Earthshine. Interestingly this was not the case for GALEX. Figure 4.3 shows the comparison between the CASTOR UV and GALEX NUV (Rodrigo et al. (2019)) filters. The local noise spectrum is also plotted in this figure to illustrate how the CASTOR filter response extends further into longer wavelengths with stronger local background. Figure 4.4 shows the comparison between the CASTOR short UV and GALEX FUV (Rodrigo et al. (2019)) filters. This show an even more extreme difference between potential UV filters. The GALEX FUV bandpass is the one that allowed the detailed measurement of the galactic UV background in Murthy (2014) because it avoids the local background. The currently proposed CASTOR Bandpasses will be more affected by local background then the bandpasses of its predecessor GALEX.
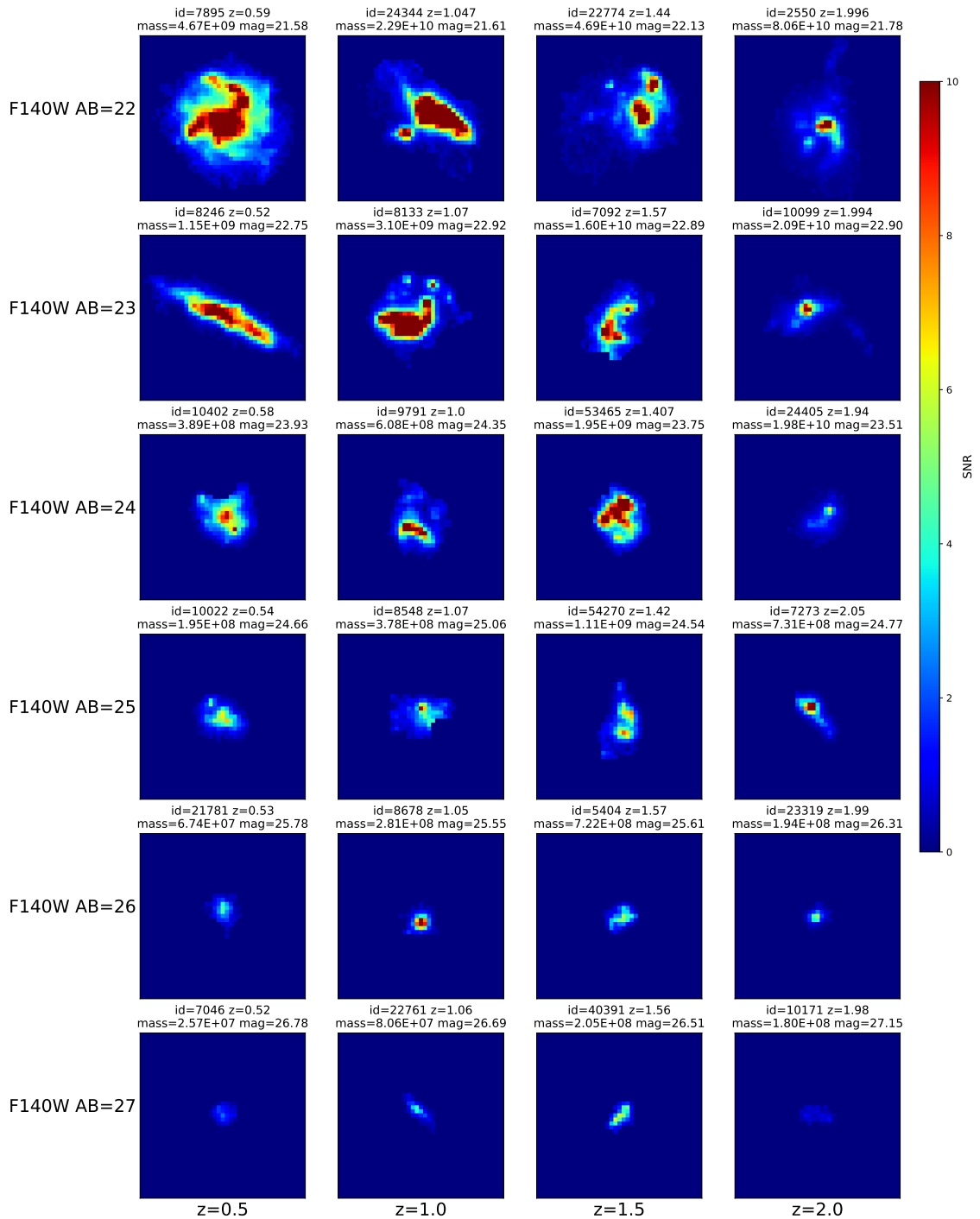
Figure 4.1: Map of the minimum SNR from CASTOR G, U and UV filters for a 100 hour observation. The galaxies images were padded to a constant field of view with an area of $24\,arcsec^2$.
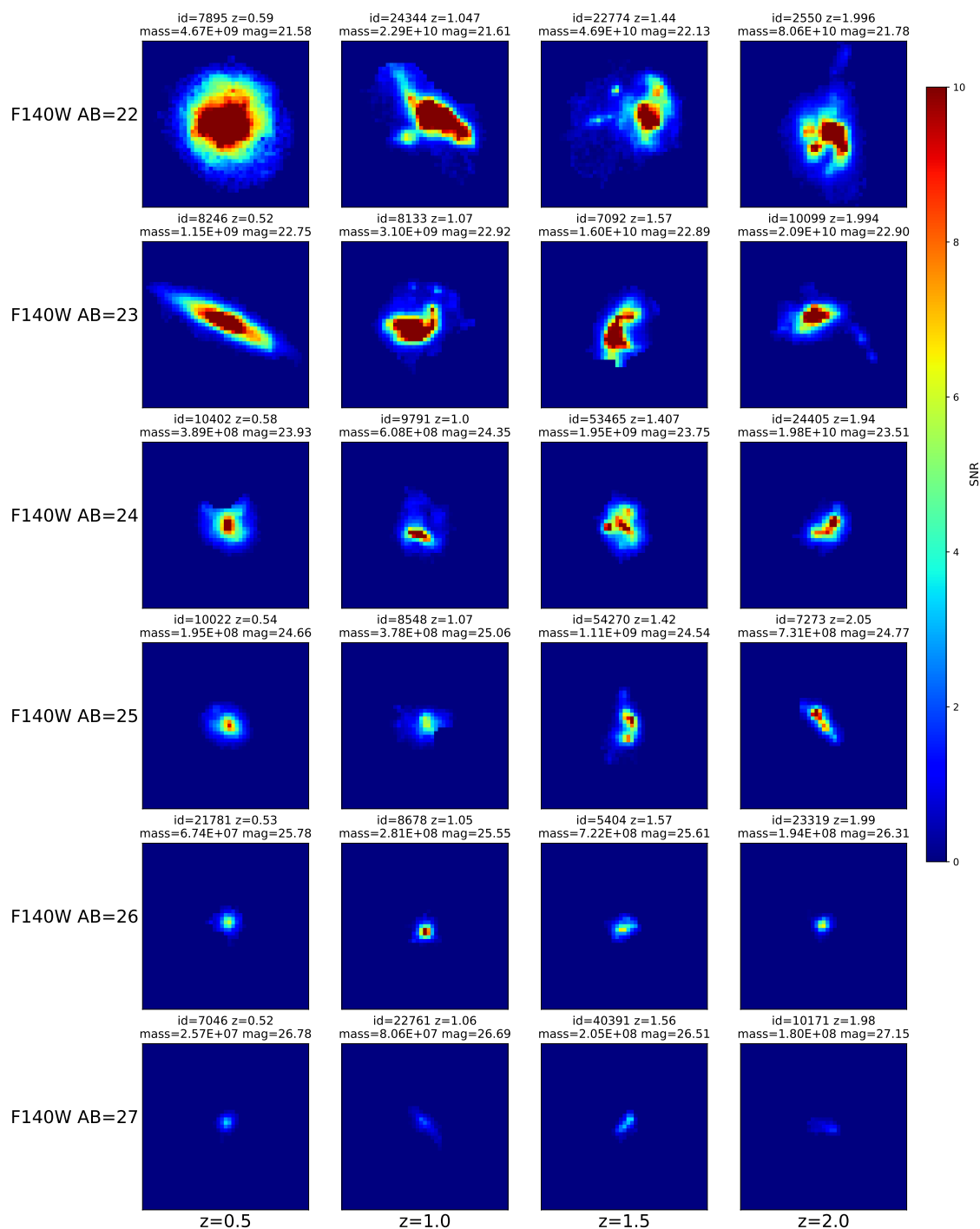
Figure 4.2: Map of the minimum SNR from all WFIRST filters for a 10 hour observation.The galaxies images were padded to a constant field of view with an area of $24\,arcsec^2$.
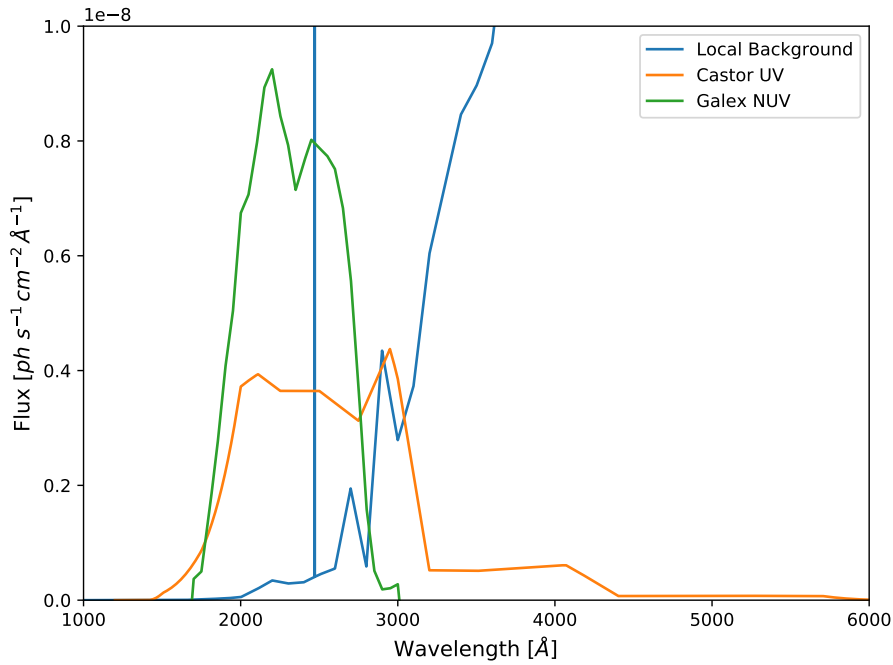
Figure 4.3: Local background spectrum with NUV filter responses for CASTOR and GALEX.
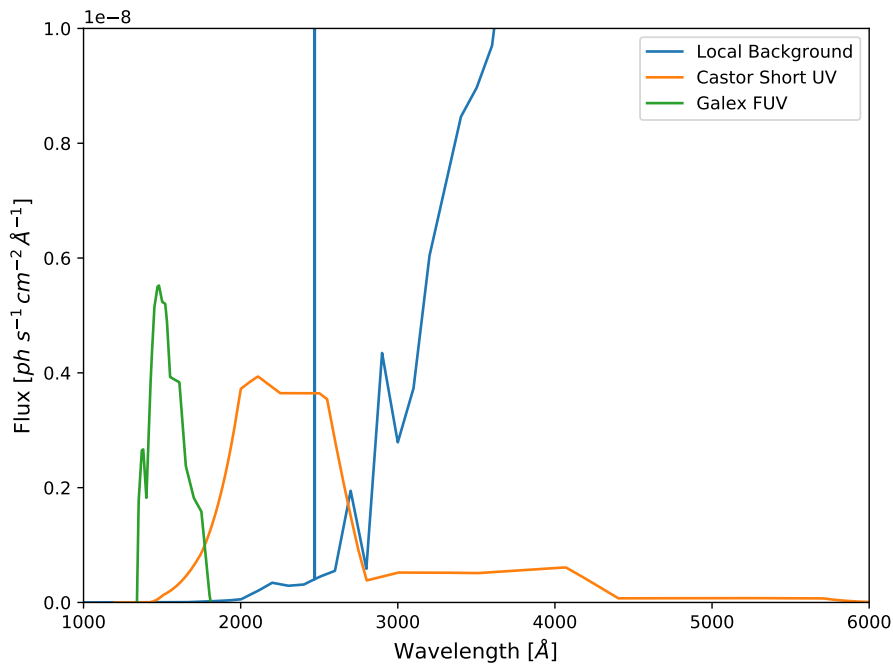

Figure 4.4: Local background spectrum with FUV filter responses for CASTOR and GALEX.

Chapter 5

Conclusions

In this work a catalogue of galactic spectra fitted to pixels in Hubble observations of the XDF was adapted to provide realistic galaxies for simulating spatially resolved images from different telescopes. Images for the XDF consisting of 4457 galaxies were simulated for CASTOR, WFIRST and Euclid response curves. A noise simulation was developed for CASTOR bandwidths and compared to WFIRST sensitivities in its bandwidths. This gives a preview of what CASTOR observations can produce. From a comparison of proposed CASTOR filters it was found that the G, U and UV filters produce the best SNR. The database and code developed while far from a fully developed tool provides the core features of an exposure simulator. A great feature of this method is the large variety of real spatially resolved galaxies that can be examined. A selection of galaxies spanning a range of magnitudes from 22-27 (F140W AB) and range of redshifts from 0.5-2.0 was examined. It was found that for objects approaching redshifts of 2.0 and magnitudes of 27 it will be difficult to do research involving spatially resolved SED fitting with 100 hour observations. While for objects with a redshift of 0.5-1.5 and magnitude of 22-25, 100 hour observations provide excellent SNR. Further, similar results will be achieved in 10 hour observations by WFIRST in its IR bandwidths.

Appendix A

Magnitude and redshift selection for all filters

The following figures are simulated image and SNR maps for the selection grid of galaxies (described in Section 4.1) for all CASTOR and WFIRST filters. For CASTOR 100 hour observations were simulated. For WFIRST shorter 10 hour observations were simulated. The galaxies images were padded to a constant field of view with an area of $24\,arcsec^2$. The figures show objects that (for the exposure times) range from easy to observe (for low redshift and brighter magnitudes) to difficult to observe (for high redshift and fainter magnitudes).
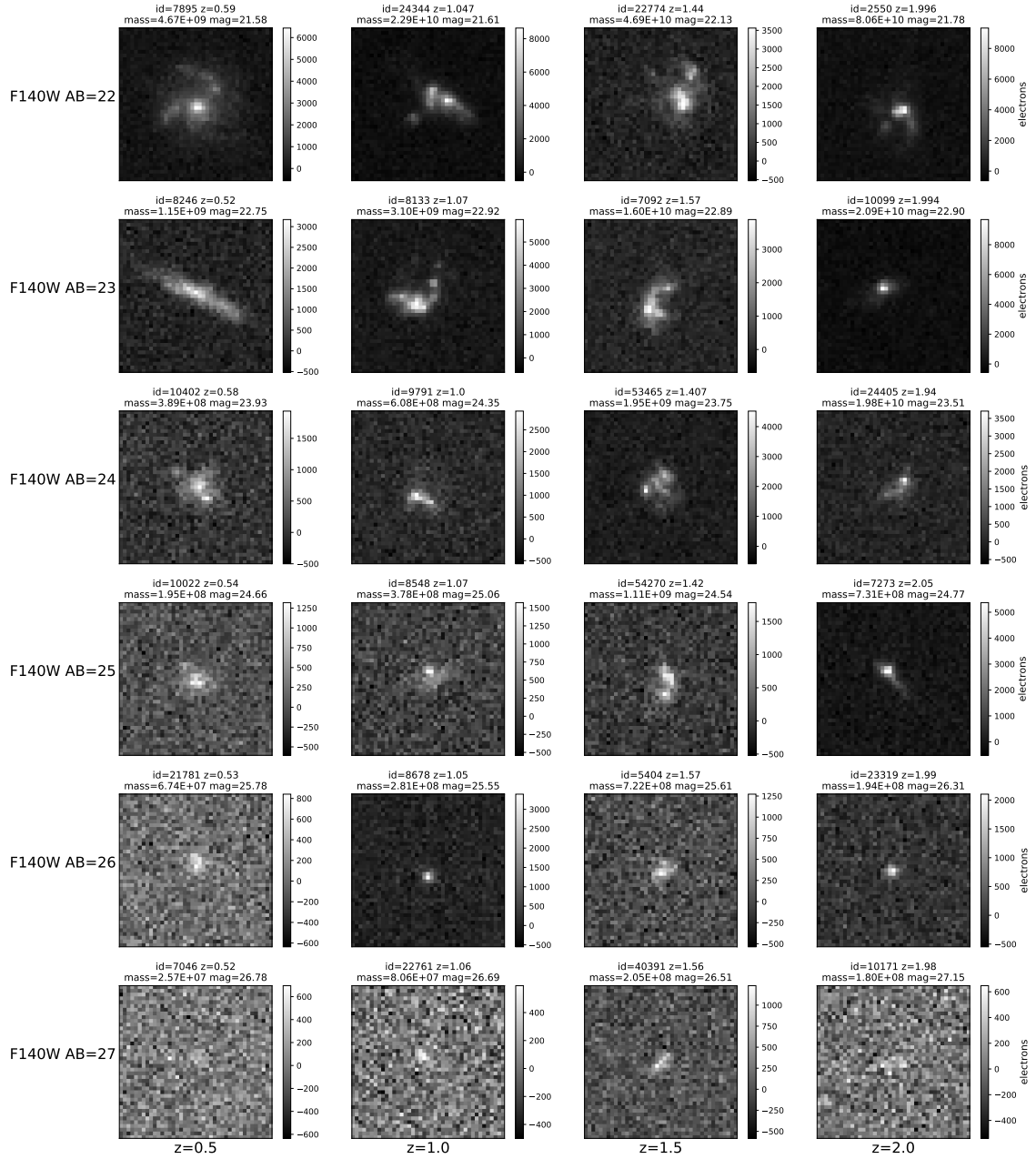
Figure A.1: Images for the selection of galaxies in CASTOR G band. The galaxies images were padded to a constant field of view with an area of $24\,arcsec^2$.
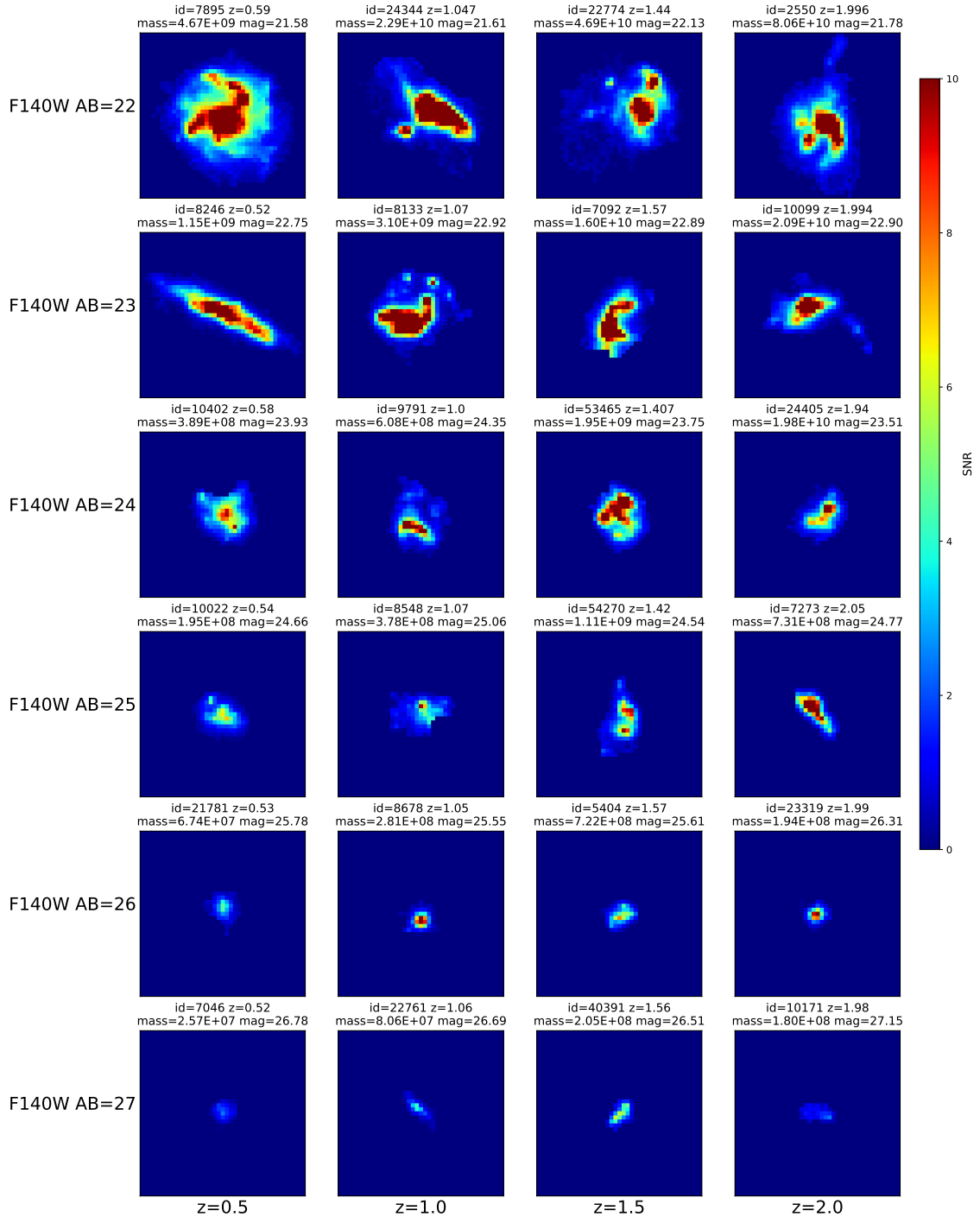
Figure A.2: SNR maps for the selection of galaxies in CASTOR G band. The colour scale reaches a maximum cut off at 10 SNR, values above that are common but clipped to make the plot more useful. The galaxies images were padded to a constant field of view with an area of $24\,arcsec^2$.
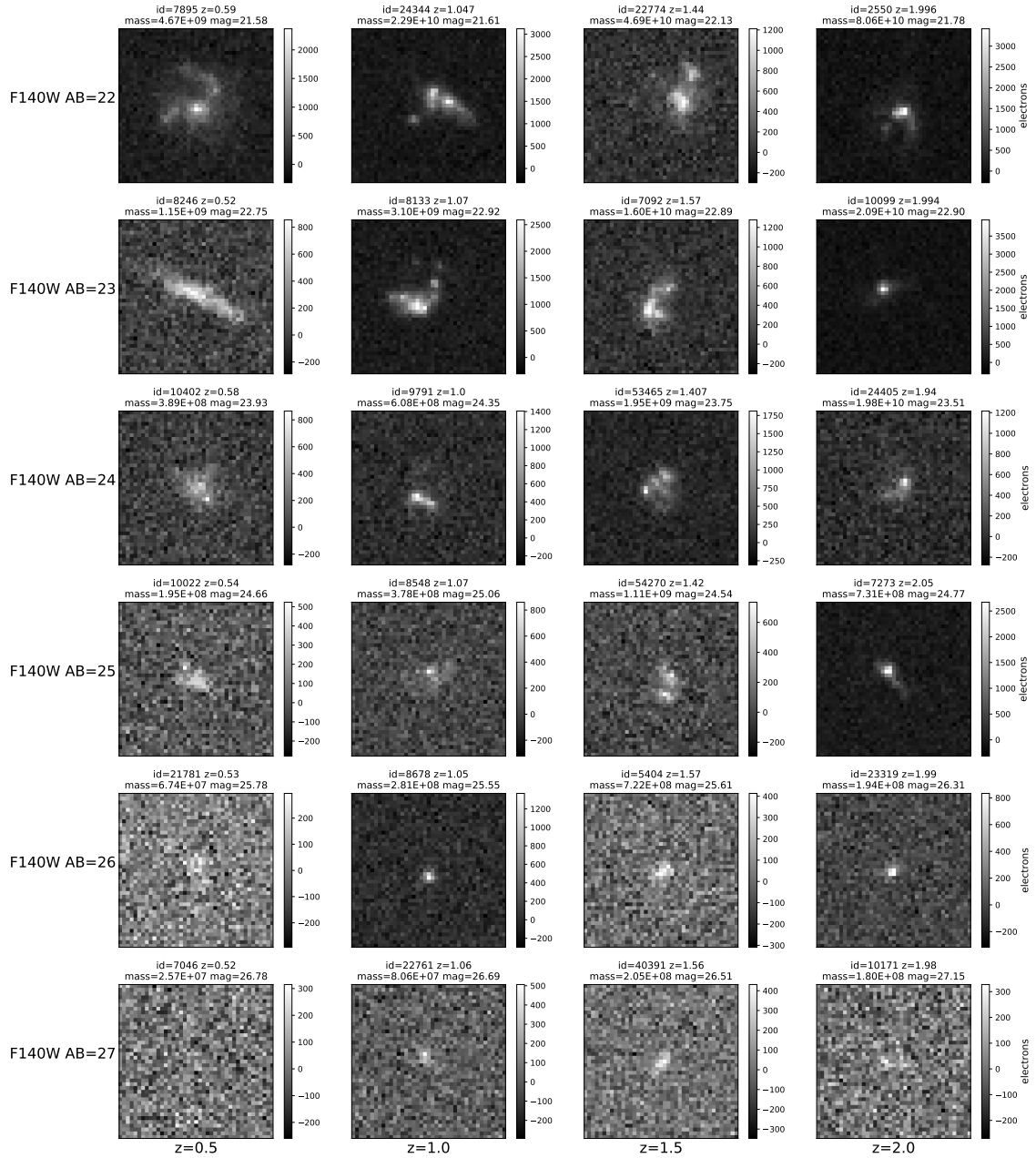
Figure A.3: Images for the selection of galaxies in CASTOR Wide U band. The galaxies images were padded to a constant field of view with an area of $24\,arcsec^2$.
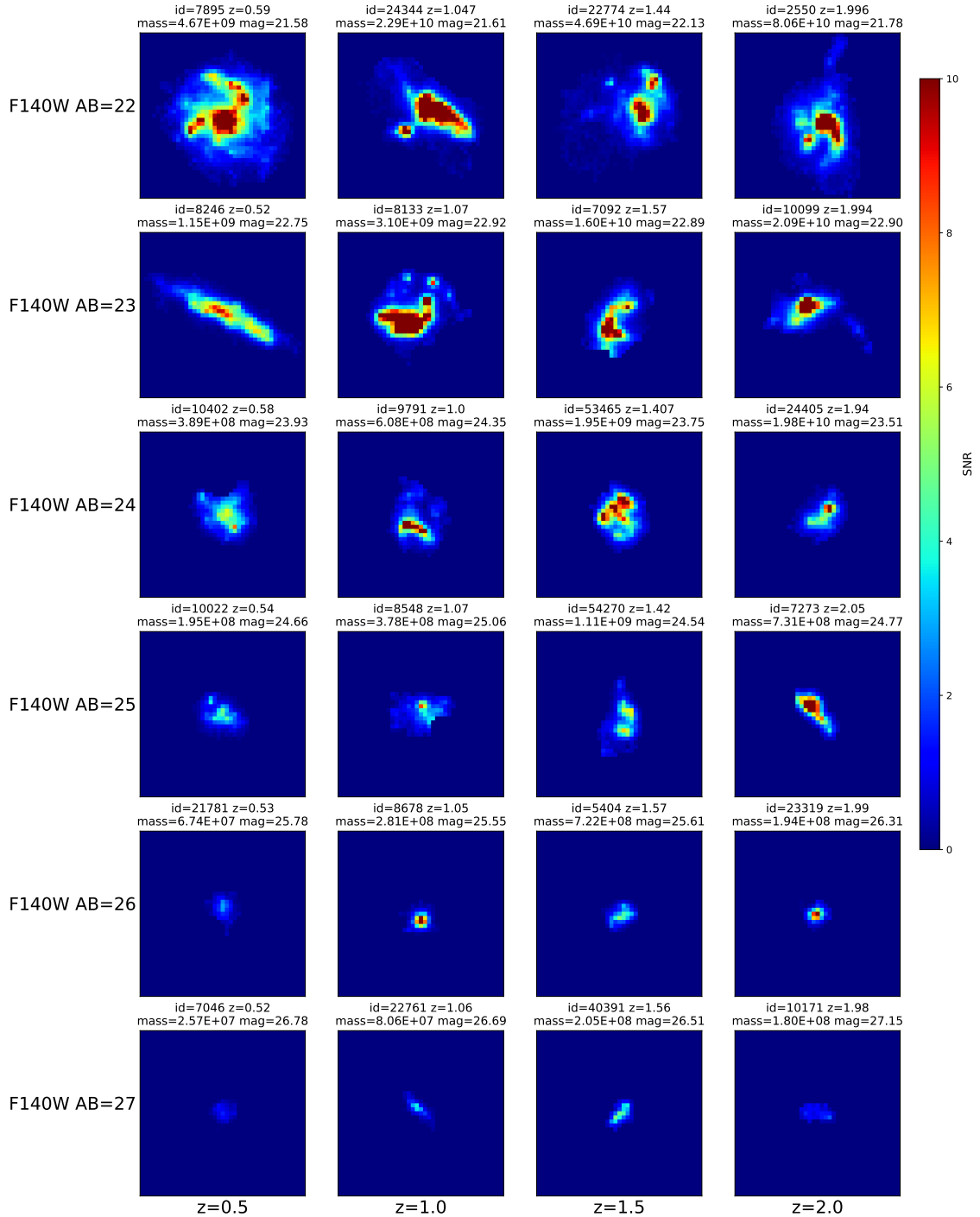
Figure A.4: SNR maps for the selection of galaxies in CASTOR Wide U band. The colour scale reaches a maximum cut off at 10 SNR, values above that are common but clipped to make the plot more useful. The galaxies images were padded to a constant field of view with an area of $24\,arcsec^2$.
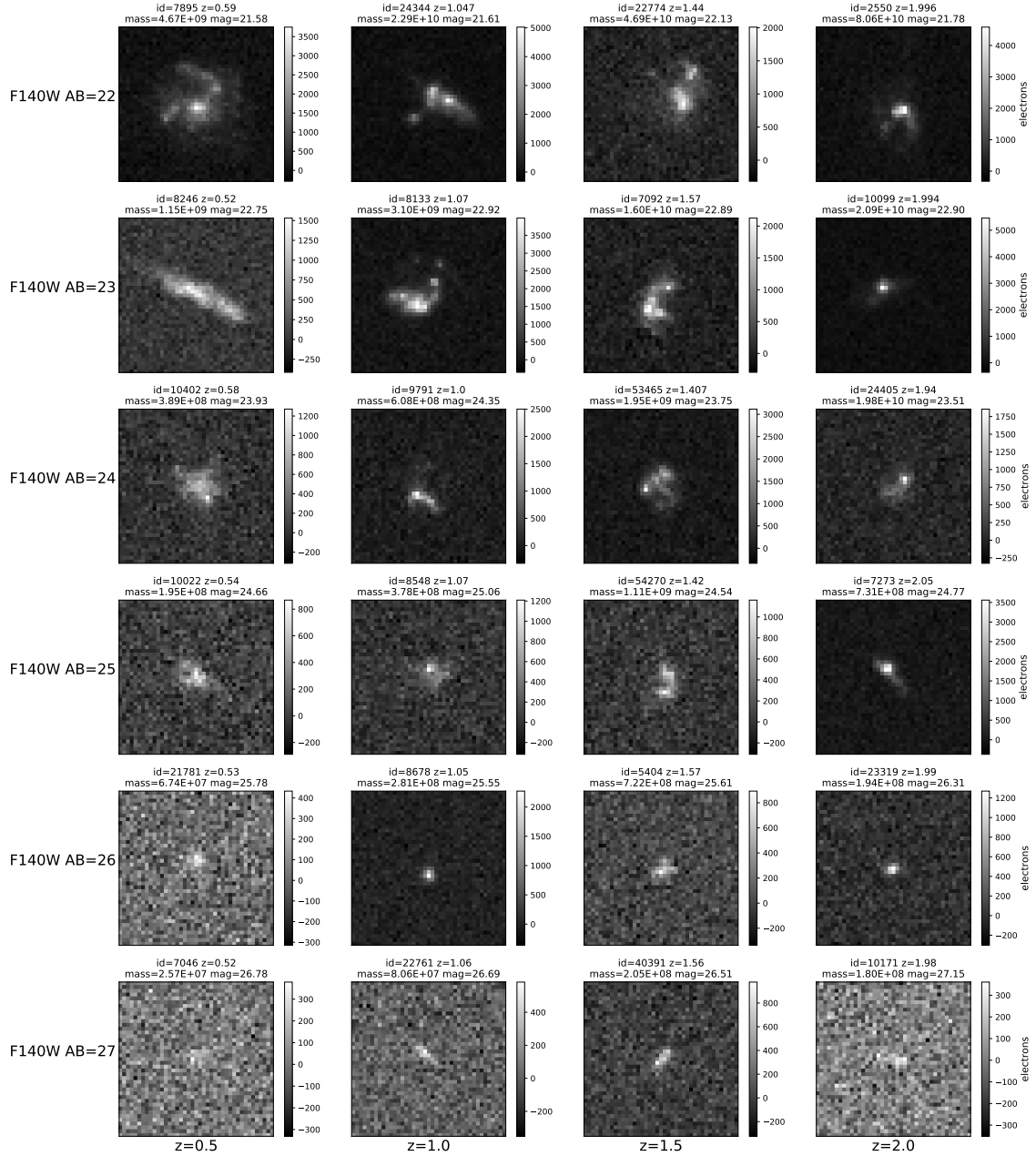
Figure A.5: Images for the selection of galaxies in CASTOR U band. The galaxies images were padded to a constant field of view with an area of $24\,arcsec^2$.

Figure A.6: SNR maps for the selection of galaxies in CASTOR U band. The colour scale reaches a maximum cut off at 10 SNR, values above that are common but clipped to make the plot more useful. The galaxies images were padded to a constant field of view with an area of $24\,arcsec^2$.

Figure A.7: Images for the selection of galaxies in CASTOR UV band. The galaxies images were padded to a constant field of view with an area of $24\,arcsec^2$.
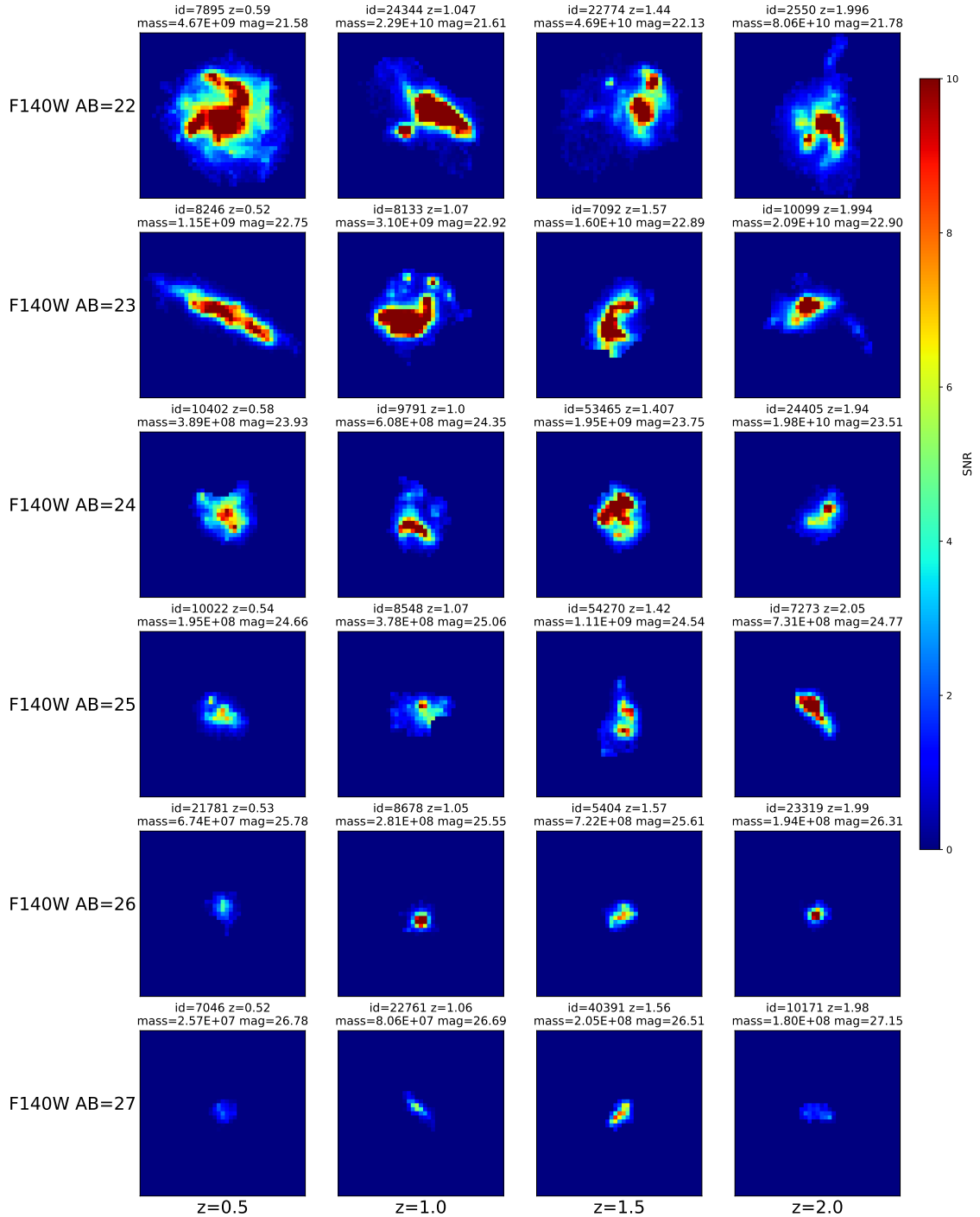
Figure A.8: SNR maps for the selection of galaxies in CASTOR UV band. The colour scale reaches a maximum cut off at 10 SNR, values above that are common but clipped to make the plot more useful. The galaxies images were padded to a constant field of view with an area of $24\,arcsec^2$.
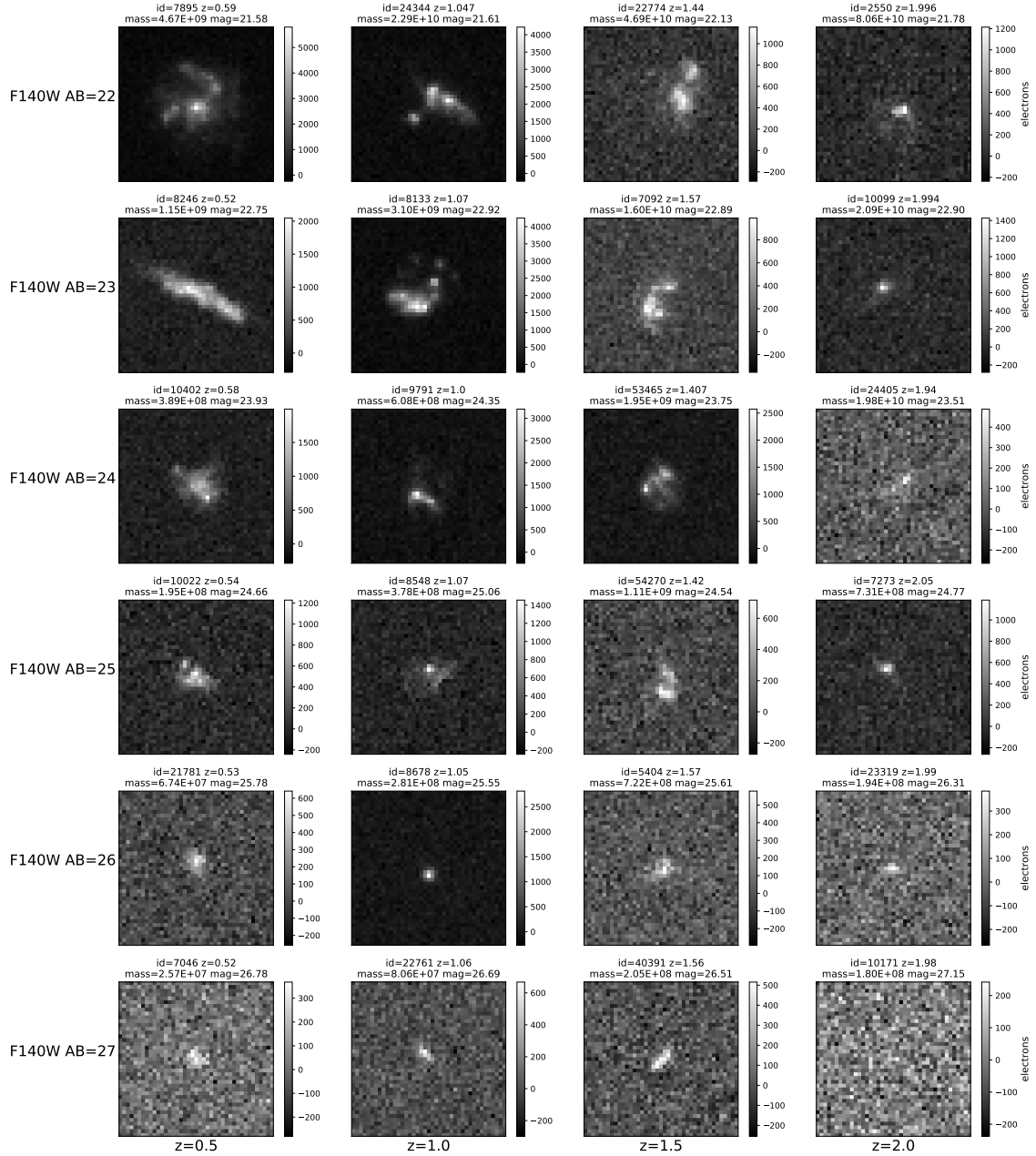
Figure A.9: Images for the selection of galaxies in CASTOR Short UV band. The galaxies images were padded to a constant field of view with an area of $24\,arcsec^2$.
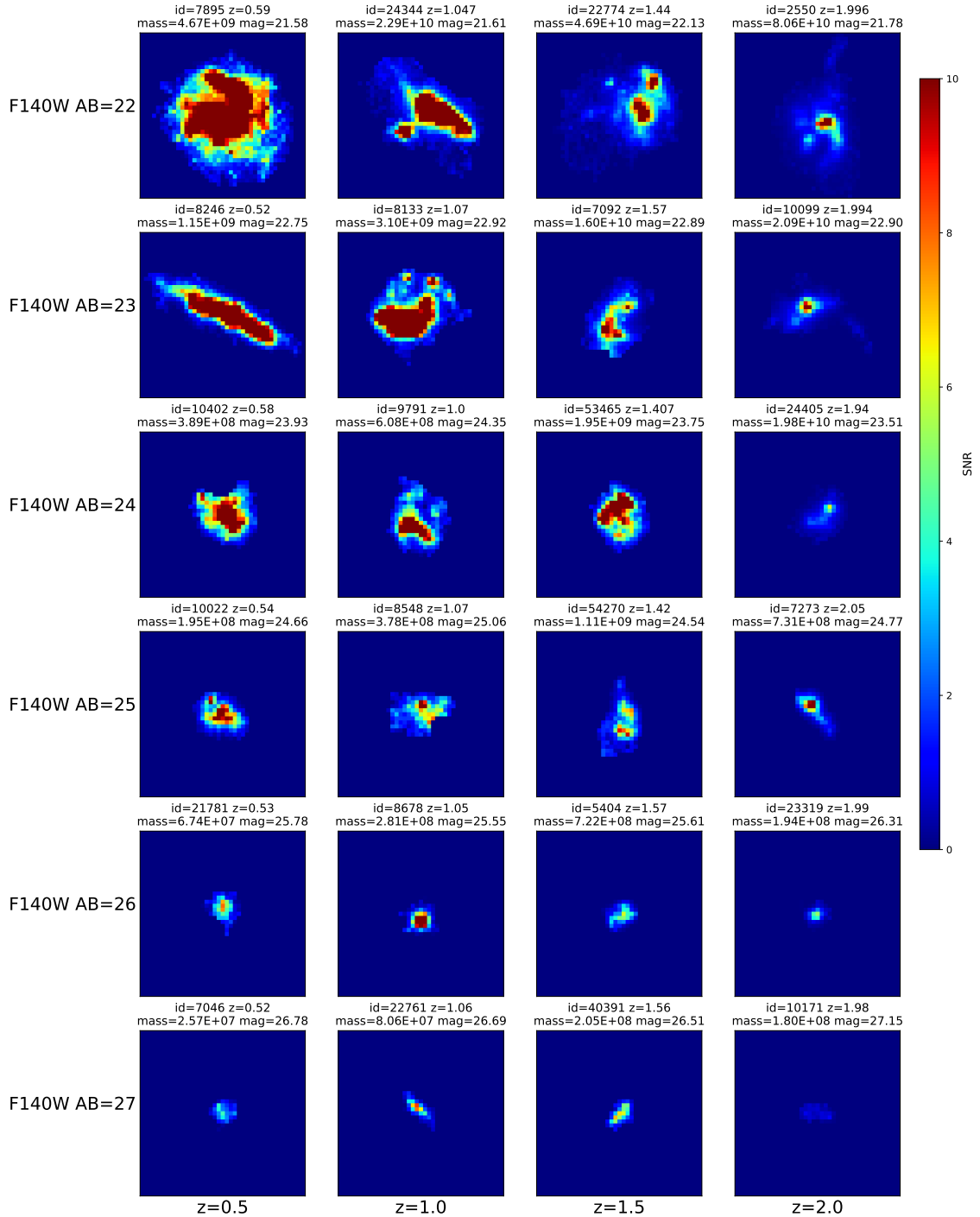
Figure A.10: SNR maps for the selection of galaxies in CASTOR Short UV band. The colour scale reaches a maximum cut off at 10 SNR, values above that are common but clipped to make the plot more useful. The galaxies images were padded to a constant field of view with an area of $24\,arcsec^2$.

Figure A.11: Images for the selection of galaxies in WFIRST F184 band. The galaxies images were padded to a constant field of view with an area of $24\,arcsec^2$.

Figure A.12: SNR maps for the selection of galaxies in WFIRST F184 band. The colour scale reaches a maximum cut off at 10 SNR, values above that are common but clipped to make the plot more useful. The galaxies images were padded to a constant field of view with an area of $24 \, arcsec^2$.
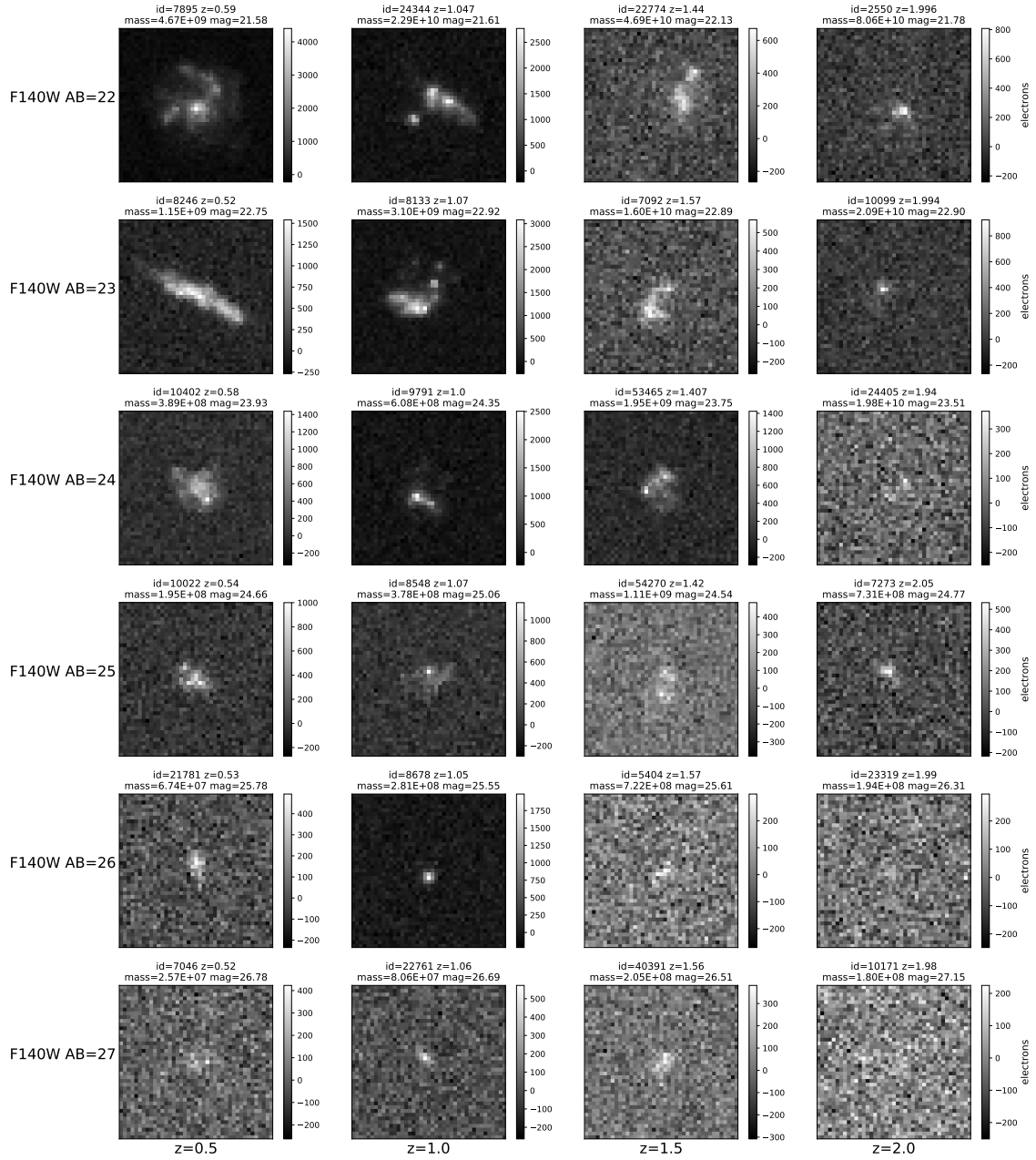
Figure A.13: Images for the selection of galaxies in WFIRST H158 band. The galaxies images were padded to a constant field of view with an area of $24\,arcsec^2$.
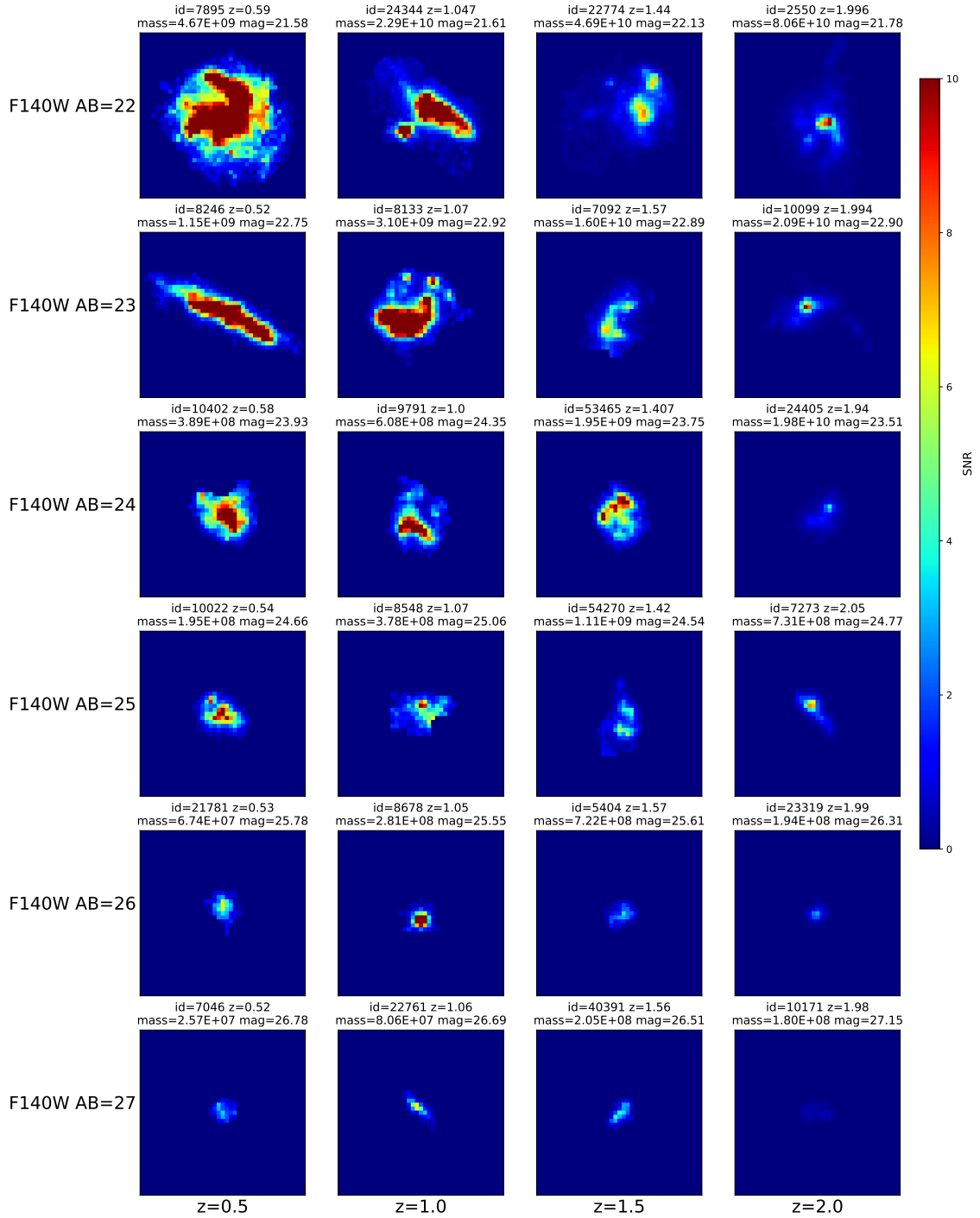
Figure A.14: SNR maps for the selection of galaxies in WFIRST H158 band. The colour scale reaches a maximum cut off at 10 SNR, values above that are common but clipped to make the plot more useful. The galaxies images were padded to a constant field of view with an area of $24\,arcsec^2$.
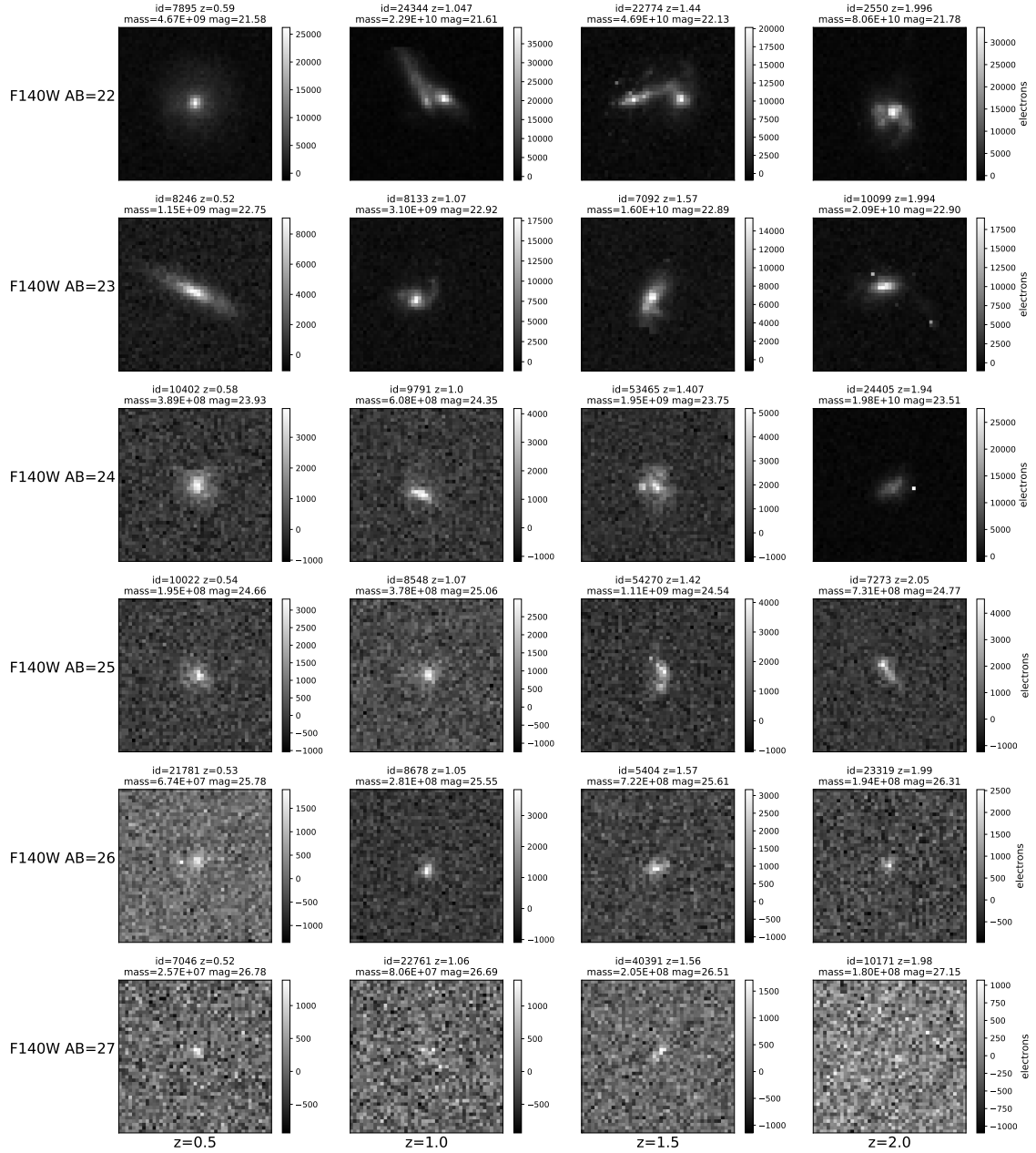
Figure A.15: Images for the selection of galaxies in WFIRST J129 band. The galaxies images were padded to a constant field of view with an area of $24\,arcsec^2$.
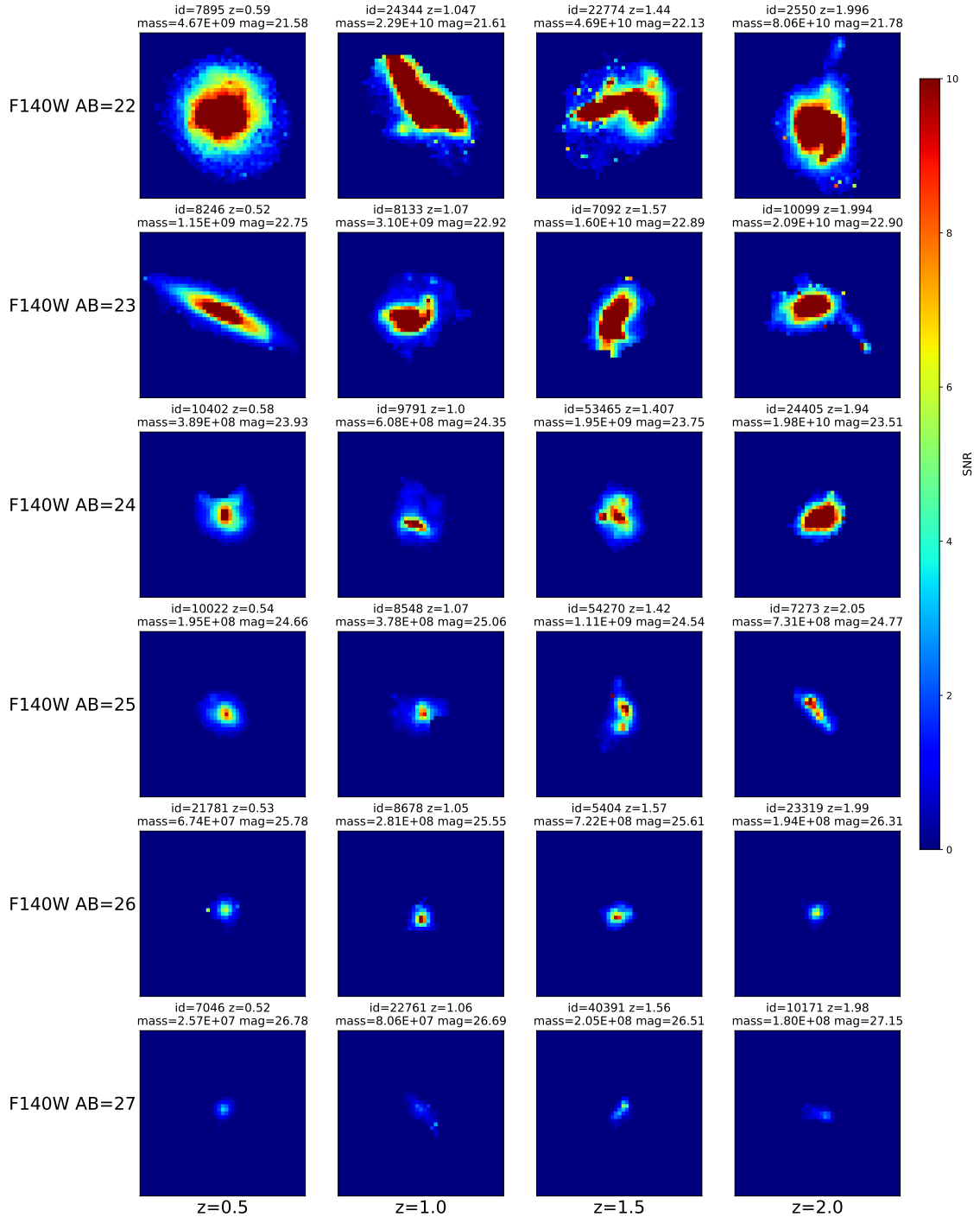
Figure A.16: SNR maps for the selection of galaxies in WFIRST J129 band. The colour scale reaches a maximum cut off at 10 SNR, values above that are common but clipped to make the plot more useful. The galaxies images were padded to a constant field of view with an area of $24 \, arcsec^2$.
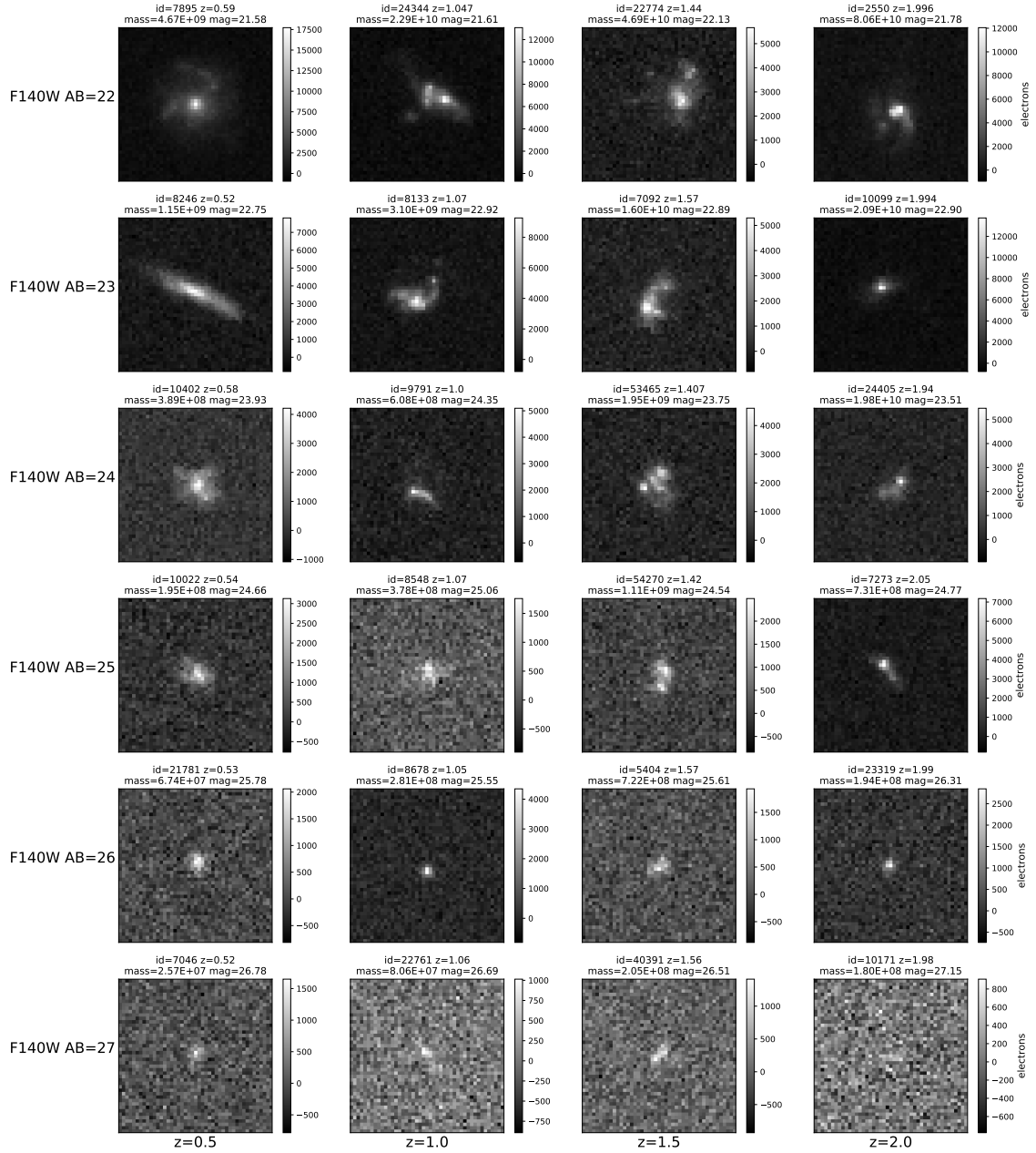
Figure A.17: Images for the selection of galaxies in WFIRST R062 band. The galaxies images were padded to a constant field of view with an area of $24\,arcsec^2$.
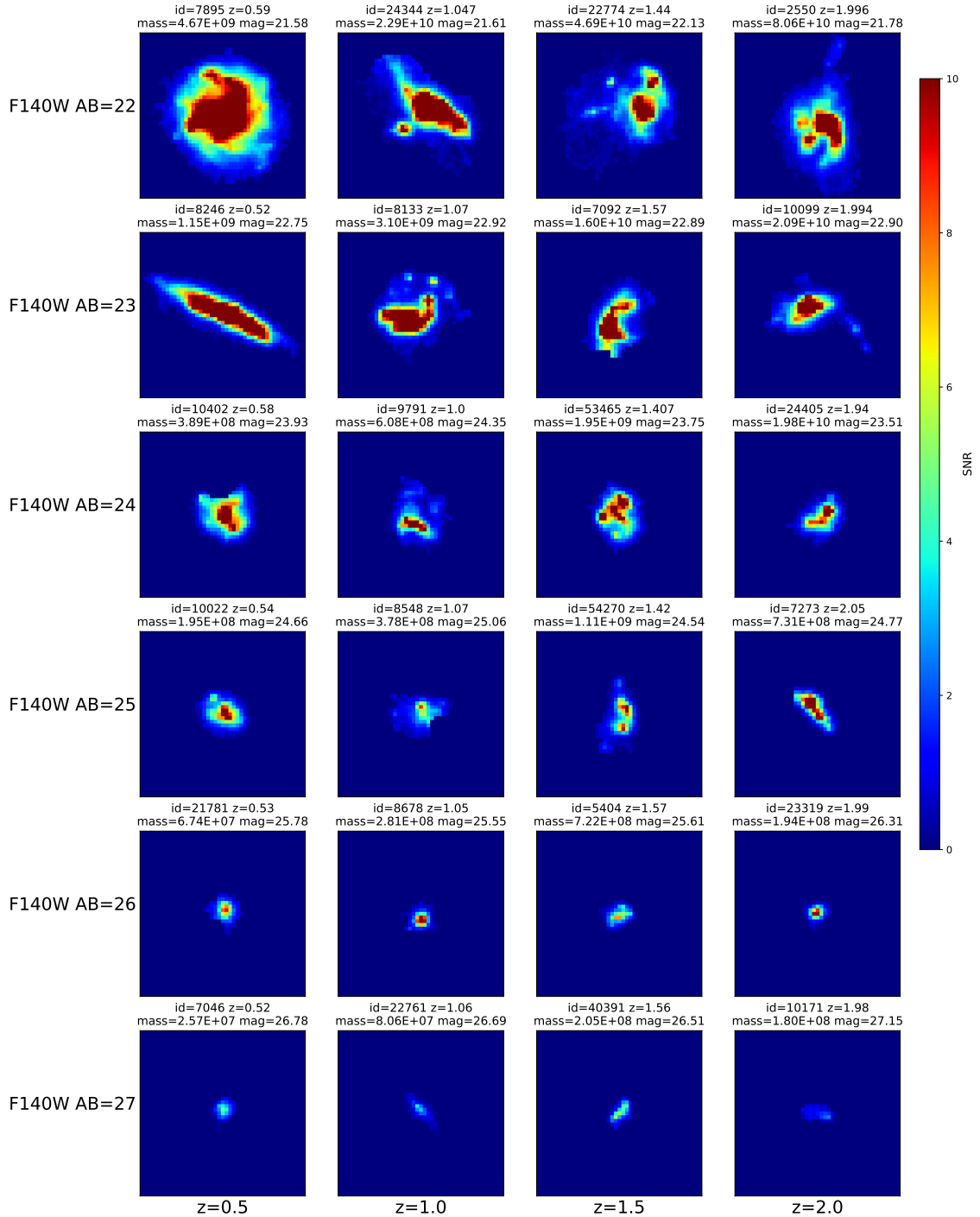
Figure A.18:   SNR maps for the selection of galaxies in WFIRST R062 band. The colour scale reaches a maximum cut off at 10 SNR, values above that are common but clipped to make the plot more useful. The galaxies images were padded to a constant field of view with an area of $24\,arcsec^2$.
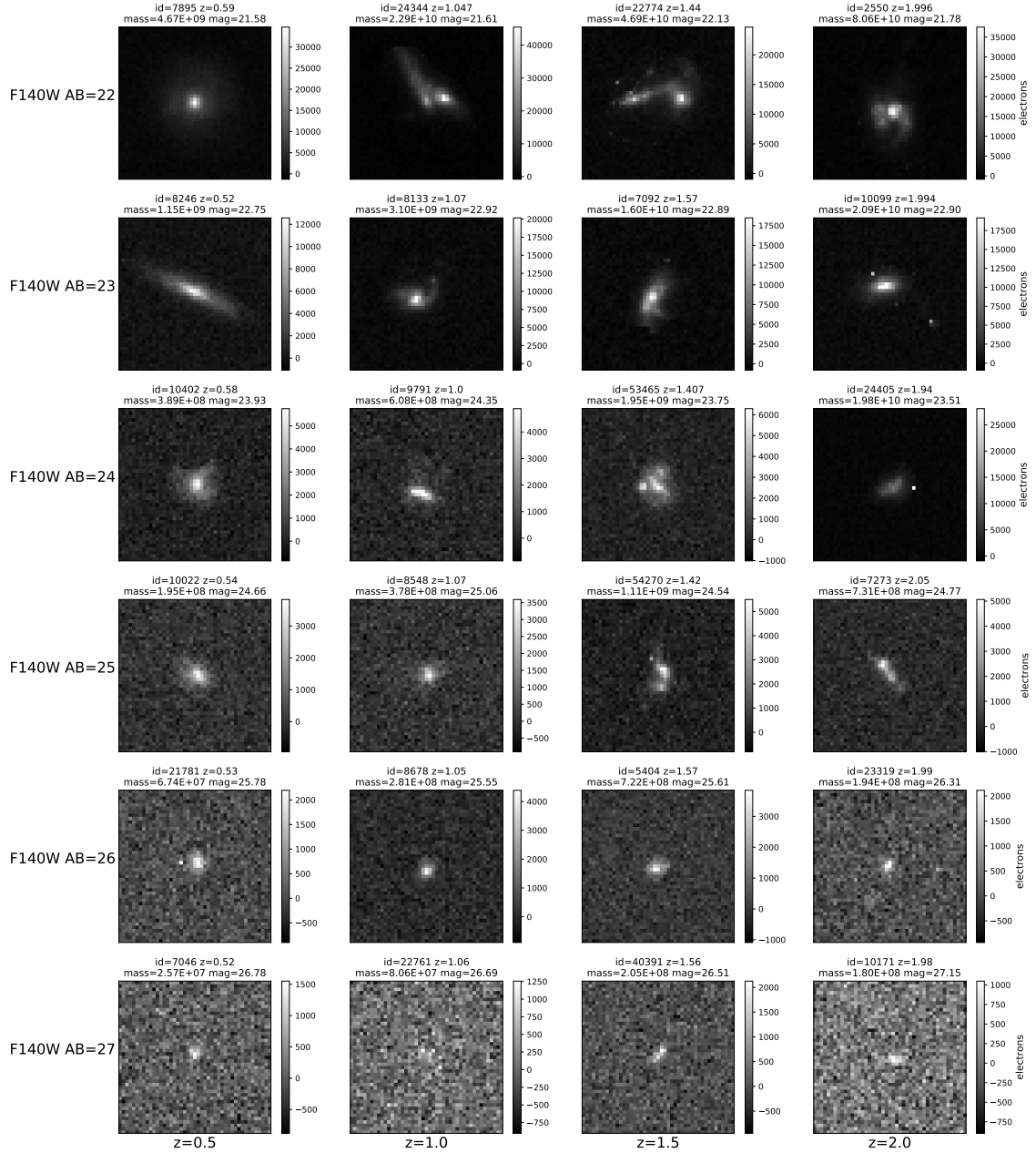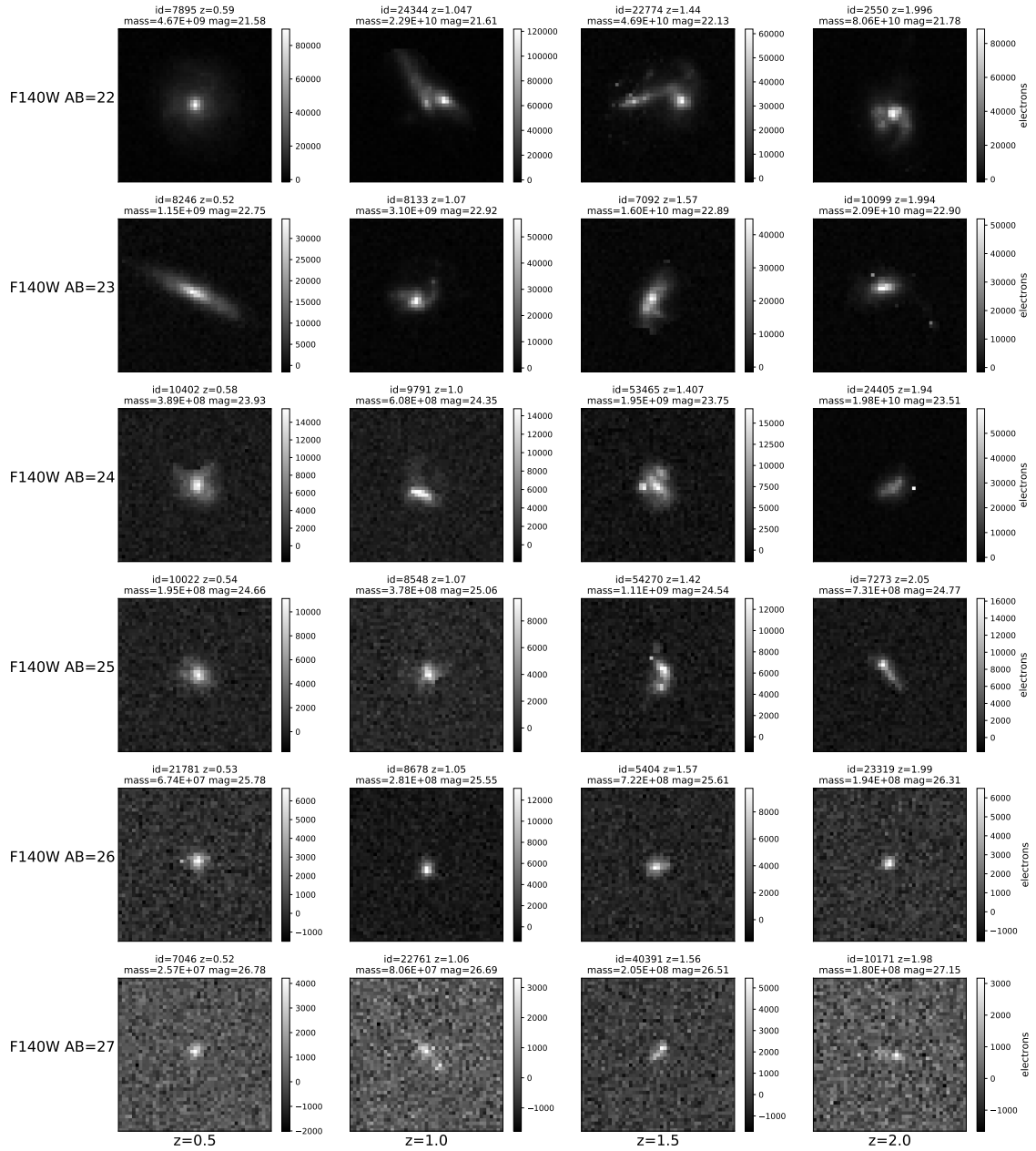
Figure A.19: Images for the selection of galaxies in WFIRST W146 band. The galaxies images were padded to a constant field of view with an area of $24\,arcsec^2$.
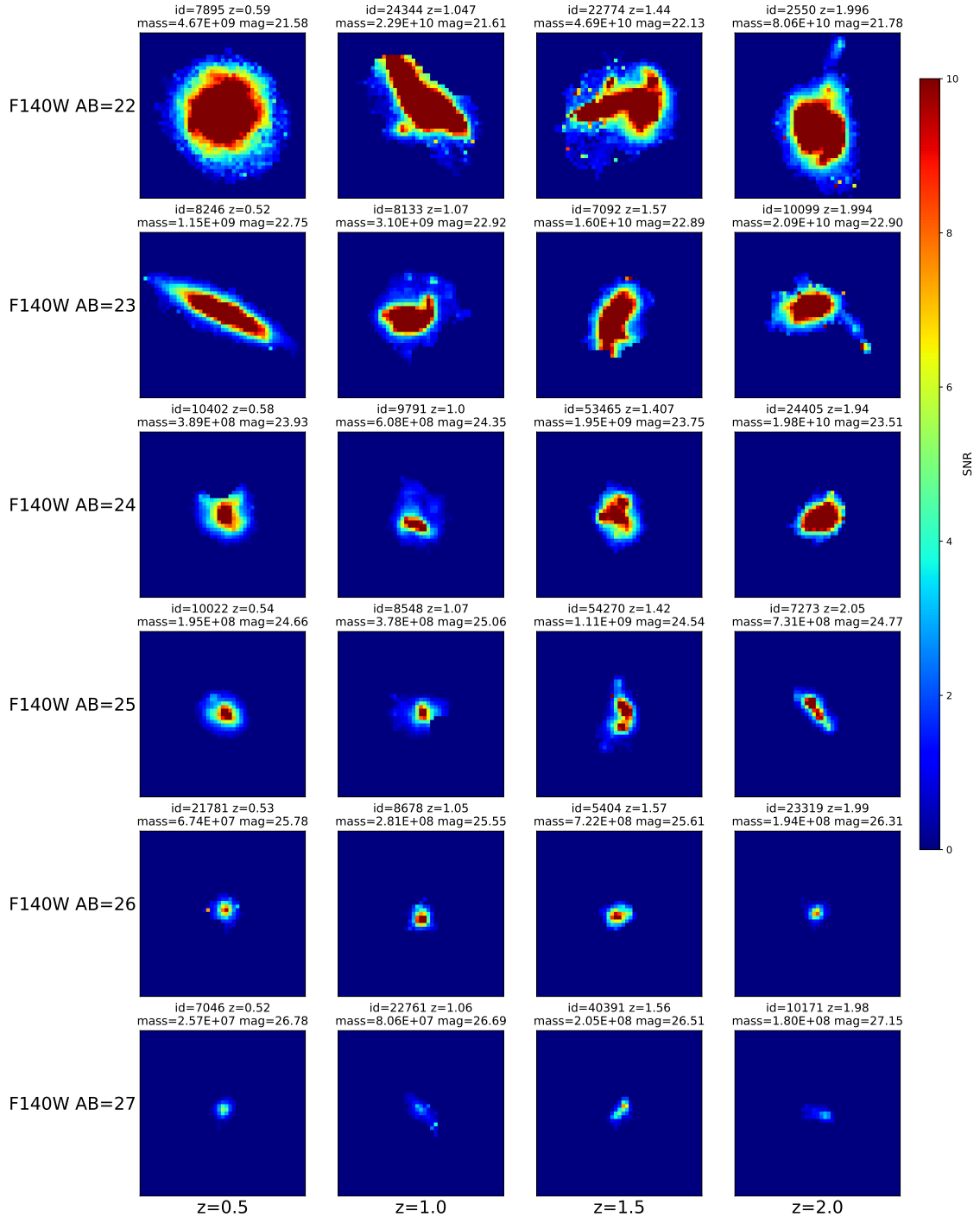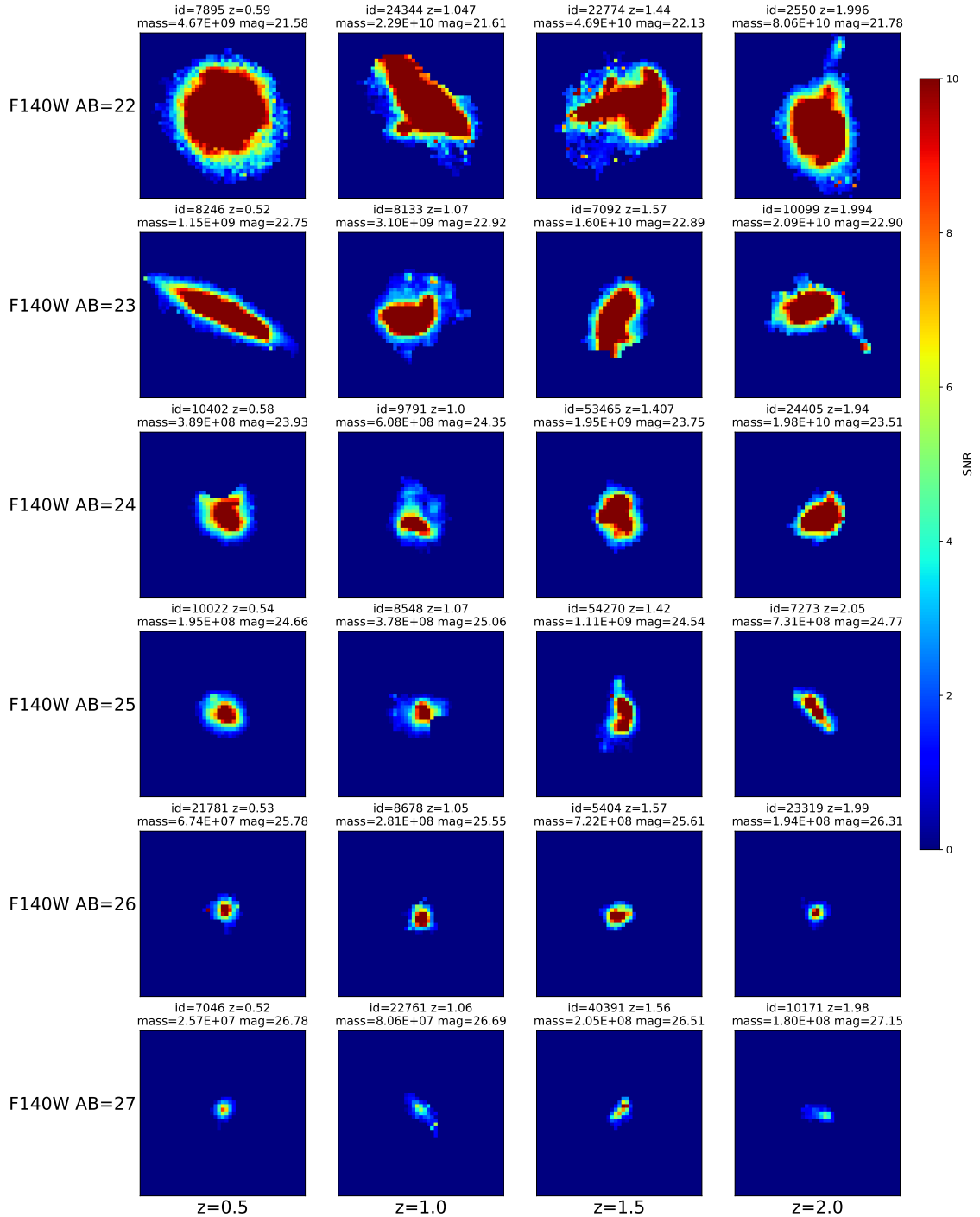
Figure A.20: SNR maps for the selection of galaxies in WFIRST W146 band. The colour scale reaches a maximum cut off at 10 SNR, values above that are common but clipped to make the plot more useful. The galaxies images were padded to a constant field of view with an area of $24\,arcsec^2$.
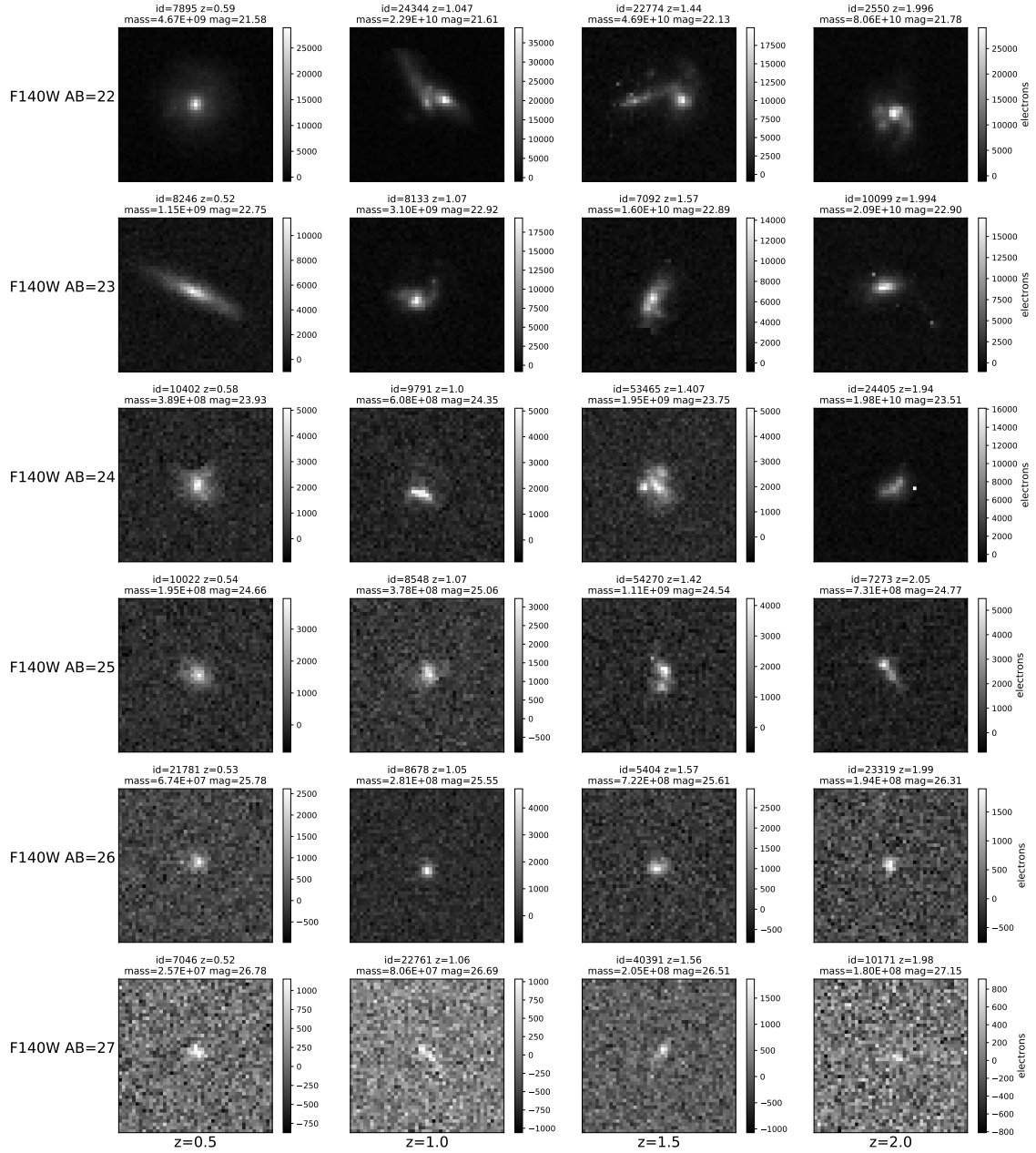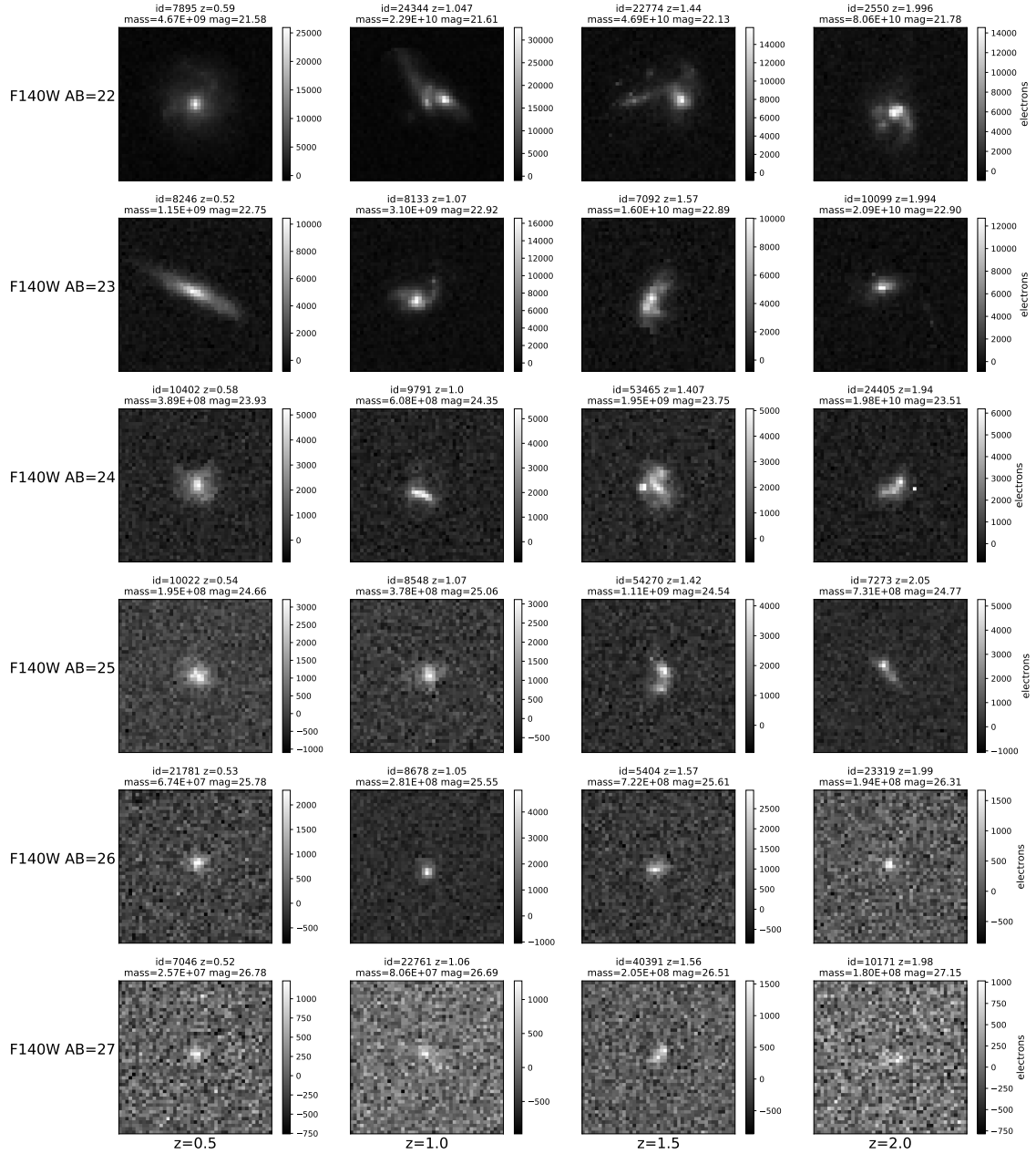
Figure A.21: Images for the selection of galaxies in WFIRST Y106 band. The galaxies images were padded to a constant field of view with an area of $24\,arcsec^2$.
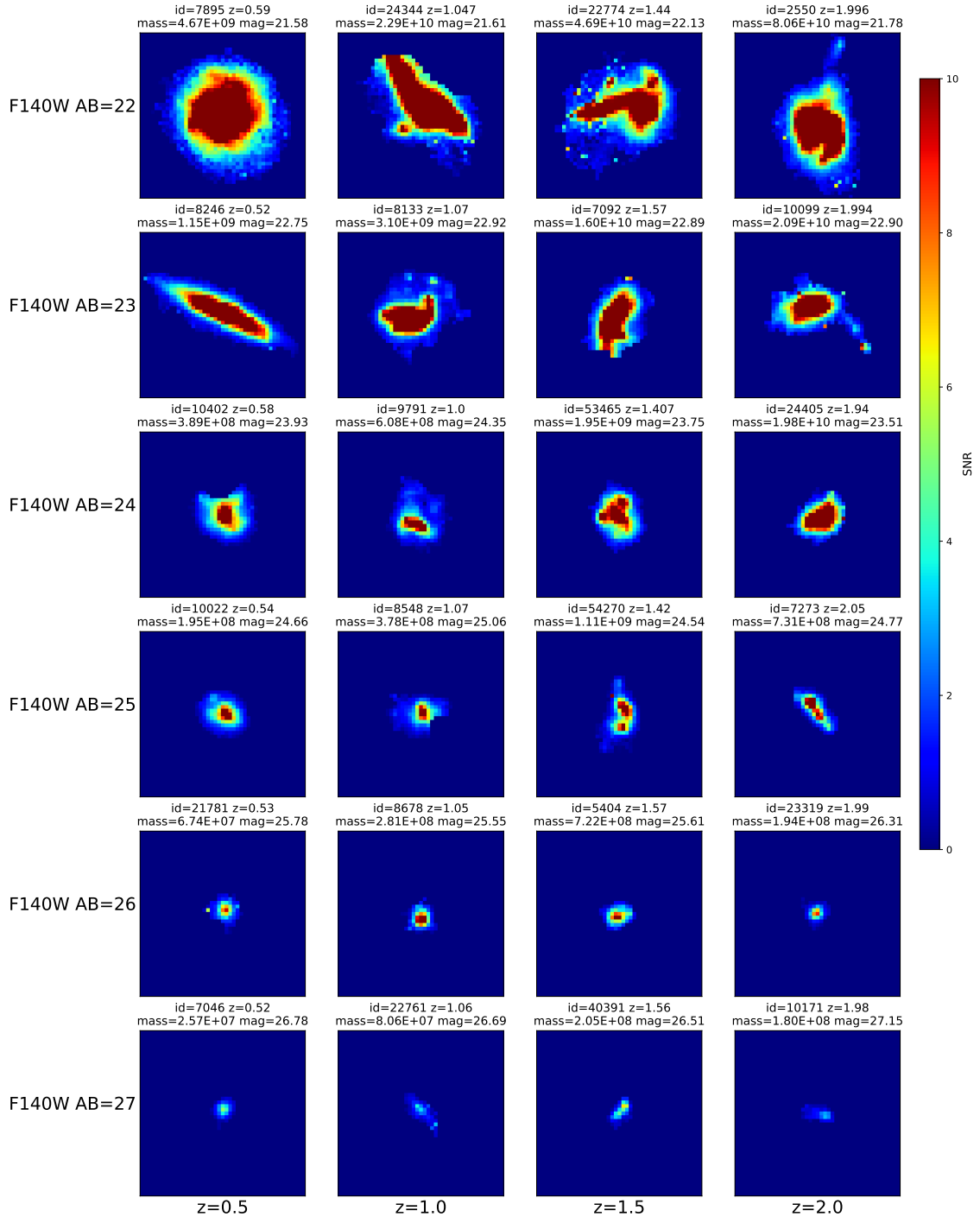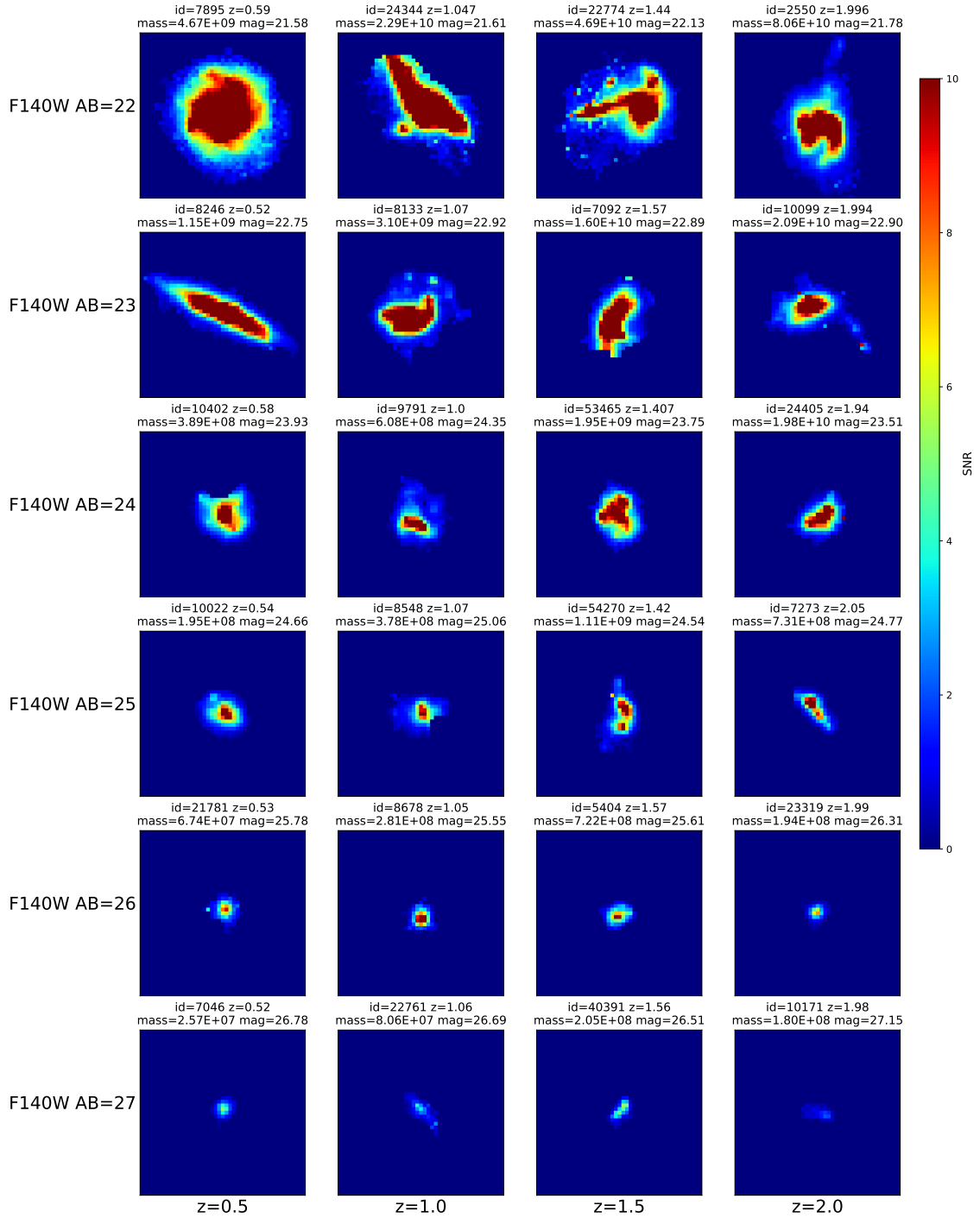
Figure A.22: SNR maps for the selection of galaxies in WFIRST Y106 band. The colour scale reaches a maximum cut off at 10 SNR, values above that are common but clipped to make the plot more useful. The galaxies images were padded to a constant field of view with an area of $24\,arcsec^2$.
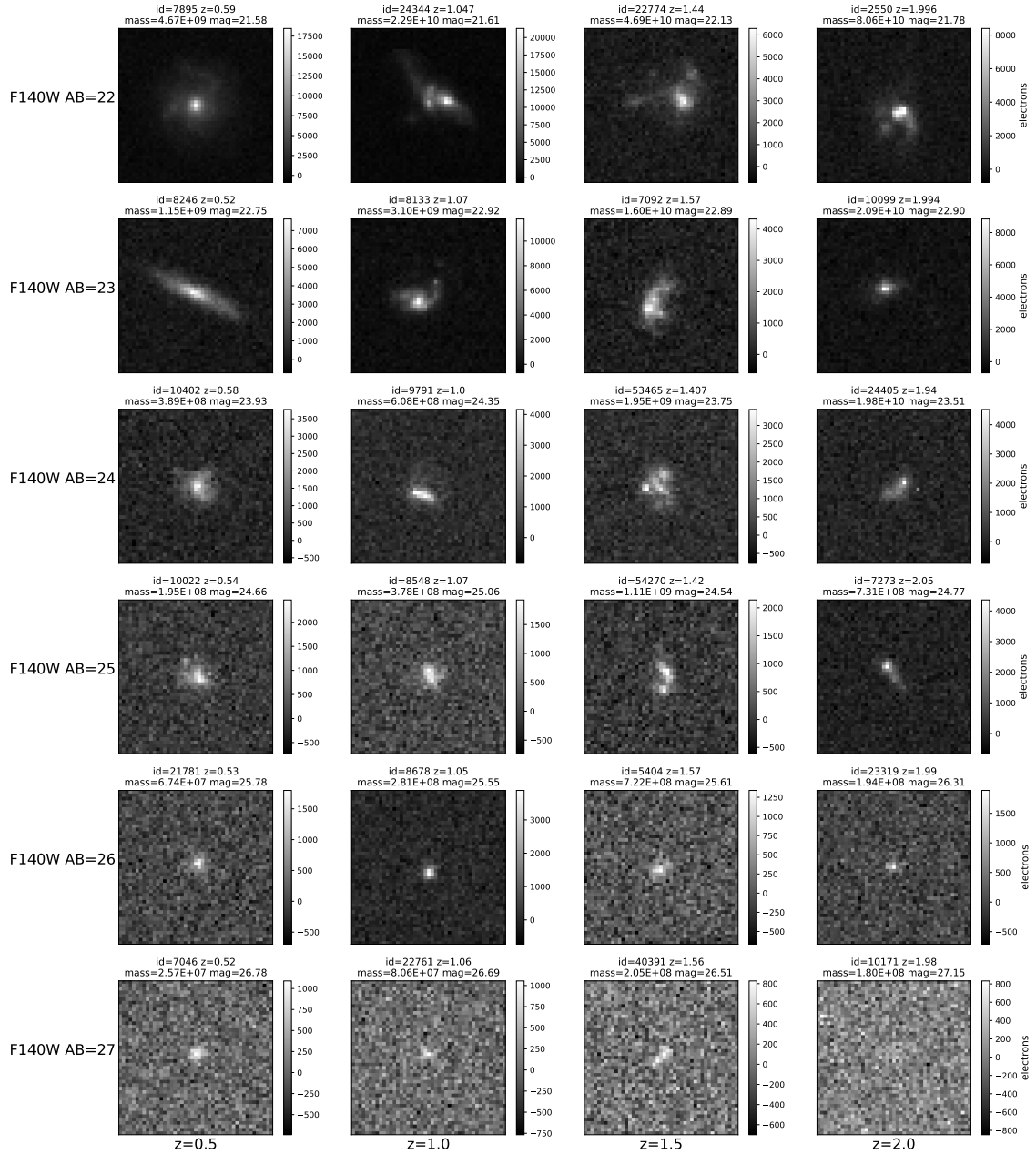
Figure A.23: Images for the selection of galaxies in WFIRST Z087 band. The galaxies images were padded to a constant field of view with an area of $24\,arcsec^2$.
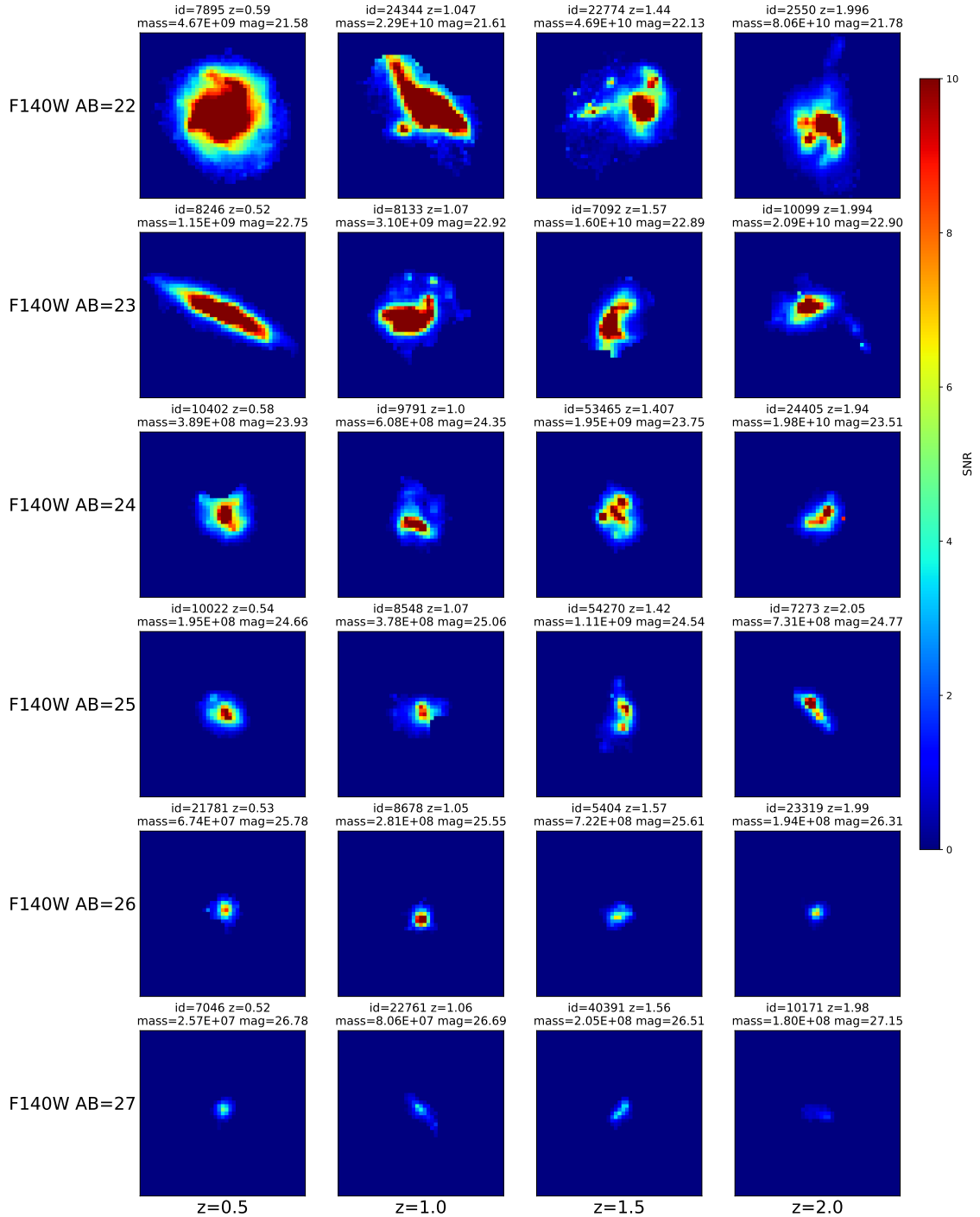
Figure A.24: SNR maps for the selection of galaxies in WFIRST Z087 band. The colour scale reaches a maximum cut off at 10 SNR, values above that are common but clipped to make the plot more useful. The galaxies images were padded to a constant field of view with an area of $24\,arcsec^2$.

Appendix B

Noise simulation code examples

```
"""This program simulates noise for CASTOR exposures.
   Author: Martin Hellmich"""


import Passband

import Resample


from random import gauss

from numpy import random, sqrt, pi, loadtxt, copy, isnan, argmin, load,
                  nansum, nanmean, nanmedian, zeros, array


def flamToPhotlam(Flam, wave):
    """Convert from Flam: : erg/sec/cm2/ to
    photlam: ph/sec/cm2/ units.
    Reference:
    https://hea-www.harvard.edu/~pgreen/figs/Conversions.pdf"""
    return 5.03e7*(Flam*wave)


def perSrToArcsec2(F):
```

```
        """Converts values that are per steradian to

        per arcseconds^2"""

        #1 steradian = 4.25 x 10^10 arcsec^2

        return F/4.25e10



# Sky Noise spectrum file (Flam: erg/sec/cm2//arcsec2)

# zodi for 30,45 (ecliptic lat,long) V = 22.1 mag arcsec2

# earthshine for 38 from the limb

skyFile = '../background/sky_spectrum.txt'



#CASTOR Values

aperture = pi*((100/2)**2) #cm^2

darkRate = 0.01 #e-/pixel/second

biasLevel = 100   #e-

readNoise = 2.9 #e-

gain = 2.0 #counts/e-

#pixel area from 2X8 sensor mosiac, 1920x5760 sensor size

#and 1378.8"x1843.2" FOV

pixelScale = 1378.8/(2*5760)

pixelArea = pixelScale**2



#resampling factor
```

```python
hubblePixScale = 0.06

factor = hubblePixScale/pixelScale


#Non local FUV values (photons cm-2 s-1 sr-1 -1)
"""Greater than 30deg galactic latitude, 300-1000 measured
by Galex (Murthy,2014)."""
galFlux = perSrToArcsec2(1000.0)
#photons cm-2 s-1 arcsec-2 -1
gale = (galFlux*pixelArea)/gain


# load sky  background spectrum,
#flux unit = erg/sec/cm2//arcsec2
skyWave, skySpec = loadtxt(skyFile,

                          unpack=True, usecols=(0,3))
# integrate over sky area assuming uniform sky background
skyFlux = skySpec*pixelArea #erg/sec/cm2/
# convert units to photlam (ph/sec/cm2/) from flam
skyPhot = flamToPhotlam(skyFlux,skyWave)
skye = skyPhot/gain
#add geocoronal emmision emission line [O II] 2471
#has a flux of 1.51015 erg cm2 s1 arcsec2
geoFlux = 1.5e-15*pixelArea
```

```python
geoWave = 2471

geoPhot = flamToPhotlam(geoFlux, geoWave)

geoe = geoPhot/gain


def gaussNoise(image, mean, sigma):

    gauss = random.normal(mean, sigma, (image.shape))

    return gauss


def plotSky():

    figure(figsize=(8,6))

    plot(skyWave, skyPhot)

    title('Sky Spectrum', fontsize=14)

    xlabel(r'Wavelength [$\AA$]', fontsize=12)

    ylabel(r'flux [photons/sec/cm2/$\AA$]', fontsize=12)


def skyCounts(pbWave, interpThroughput, expTime):

    """"Returns Sky counts and associated poisson noise

    for a given filter bandpass."""

    #interpolate flux to 1 angstrom resolution on filter range

    interpFlux = Passband.interpolateAngstrom(pbWave,

                                              skyWave, skye)
```

```python
    #adding geocoronal line after interpolation

    geoBin = argmin(abs(pbWave - geoWave))


    #calculated flux passed by filter

    filterflux = nansum(interpFlux*interpThroughput)

                       + geoe*interpThroughput[geoBin]


    skyCounts = filterflux*aperture*expTime


    # poisson uncertanty in the sky

    skyNoise = sqrt(skyCounts)


    return skyCounts, skyNoise


def galCounts(pbWave, interpThroughput, expTime):
    """Returns counts and associated poisson noise

    for a given filter bandpass.

    Galaxy noise is a constant function for now."""


    # flux with telescope response

    filterflux = gale*nansum(interpThroughput)

    counts = filterflux*aperture*expTime
```

```python
    # poisson uncertanty

    noise = sqrt(counts)


    return counts, noise



def darkCounts(expTime):

    """Calculates dark current counts and noise"""

    darkCounts = darkRate * expTime

    darkNoise = sqrt(darkCounts)

    return darkCounts, darkNoise



filterPath = '../passbands/'

filePath = '/Users/martin/cleanimage/'

filterList = ['CASTOR_g', 'CASTOR_u', 'CASTOR_u300_400',

              'CASTOR_uv135_260', 'CASTOR_uv150_300']

exposureList = [1,10,100,1000]


def padImage(image, shape):

    image2 = zeros(shape)

    offset = (array(shape) - array(image.shape))/2.0

    opposite = offset + array(image.shape)
```

```python
    image2[int(offset[0]):int(opposite[0]),

            int(offset[1]):int(opposite[1])] += image

    return image2



def simNoise(galaxyID, filt, exp, padShape=None):

    '''Simulates noise frames for a given filter (0-4)

    and exposure time (0-3)'''



    file = filePath+str(galaxyID)+'_'+filterList[filt]+'_phot.npy'

    pbWave, interpThroughput = Passband.passband(filterPath

                                    +filterList[filt]+'.dat')



    #name to save files

    tag = (file.split('/')[-1]).split('.')[0][0:-5]



    #exposure time is in hours!

    exph = exposureList[exp]

    expTime = exph*3600 #hours to seconds



    #load image in photons/s/cm2

    hubbleImage = load(file)

    #resample
```

```
castorImage = Resample.resample(hubbleImage, factor)

#pad image

if (padShape != None):

    castorImage = padImage(castorImage, padShape)

#convert to counts

counts = (castorImage*expTime*aperture)/gain


#relpace nans

clean = copy(counts)

clean[isnan(clean) == True] = 0


#simulate noises

darkcounts, darknoise = darkCounts(expTime)

skycounts, skynoise = skyCounts(pbWave, interpThroughput, expTime)

galcounts, galnoise = galCounts(pbWave, interpThroughput, expTime)


#mean noise

sigma = sqrt(nanmedian(counts)+darkcounts+readNoise**2

                    +skycounts+galcounts)

#signal to noise map

snr = clean/sigma
```

```
simnoise = gaussNoise ( counts ,0 , sqrt ( nanmedian ( counts )

    +darkcounts+readNoise**2+skycounts+galcounts ) )

combinednoise = clean + simnoise


return combinednoise , snr
```

Appendix C

Bandpass model code examples

```python
"""Calculates AB magnitude from spectrum and bandpass
    in fnu units.
    Author: Martin Hellmich"""


# import relevent packages
from numpy import arange, log10, loadtxt, round, argmin,
        pi, multiply, nan, nansum
from scipy.interpolate import interp1d
from pysynphot import ObsBandpass


wfirstQE = loadtxt(".../wfirst/h2rg.txt", unpack=True)
wfirstWave = wfirstQE[0]  #angstrom
wfirstThroughput = wfirstQE[1]


def fnuToPhotlam(Fnu, wave):
    """Convert from Fnu to photlam units.
    Reference:
    https://hea-www.harvard.edu/~pgreen/figs/
```

```python
    Conversions.pdf"""
    return  1.51e26*(Fnu/wave)



def waveCut(lowcut, highcut):
    """Array for wavelength range"""
    wavecut = arange(lowcut, highcut+1,1)
    return wavecut



def interpolateAngstrom(wavecut, wave, flux):
    '''Interpolate to 1 angstrom resolution on
    wavelength subset'''
    Spectrum = interp1d(wave, flux, bounds_error=False,
        fill_value=nan)
    interpFlux = Spectrum(wavecut)
    return interpFlux



def passband(file):
    """Load passband in angstrom from text file
        and interpolate."""
    # load passband
    passband = loadtxt(file, unpack=True)
    wavelength = passband[0]
```

```
        throughput = passband[1]


        #interpolate to 1 angstrom
        pbWave = waveCut(min(wavelength),max(wavelength))
        interpThroughput = interpolateAngstrom(pbWave,wavelength,
            throughput)


        return pbWave, interpThroughput


def pysynphotBP(tagString):
    """Load load hubble bandpass from pysynphot and
    interpolate.
    acs,wfc1: f435w, f606w, f775w, f814w, f850lp
    wfc3,ir: f105w, f125w, f140w, f160w"""
    # load passband
    bp = ObsBandpass(tagString)
    wavelength = bp.wave
    throughput = bp.throughput


    #interpolate to 1 angstrom
    pbWave = waveCut(min(wavelength),max(wavelength))
    interpThroughput = interpolateAngstrom(pbWave,
```

```
            wavelength, throughput)


    return pbWave, interpThroughput


def wfirstBand(file):
    """"Load WFIRST passband in angstrom from text file
    and interpolate."""
    # load passband
    passband = loadtxt(file, unpack=True)
    wavelength = passband[0]
    throughput = passband[1]


    #interpolate to 1 angstrom
    pbWave = waveCut(min(wavelength),max(wavelength))
    interpThroughput = interpolateAngstrom(pbWave,wavelength,
        throughput)
    interpQE = interpolateAngstrom(pbWave,wfirstWave,
        wfirstThroughput)


    transmission = 1.0


    return pbWave, interpThroughput*interpQE*transmission
```

```python
def modelFlux(pbWave, interpThroughput, wave, flux):
    """Model the flux density of the observation
    with selected band pass.
    For use in calbration."""


    #interpolate flux to 1A resolution on filter range
    interpFlux = interpolateAngstrom(pbWave, wave, flux)


    #calculated flux passed by filter
    modelflux = nansum(interpFlux*interpThroughput*pbWave)
        /nansum(interpThroughput*pbWave)


    return modelflux


def modelPhot(pbWave, interpThroughput, wave, flux):
    """Model the photons of the fnu observation
    with selected band pass.
    For use in simming images."""


    #convert ergs to photons at each wavelength
    phot = fnuToPhotlam(flux, wave)
```

```python
    #interpolate flux to 1A resolution on filter range
    interpPhot = interpolateAngstrom(pbWave, wave, phot)


    #calculated flux passed by filter
    modelPhot = nansum(interpPhot*interpThroughput)


    return modelPhot


def intFlux(pbWave, interpThroughput, wave, flux):
    """Model the integrated flux of the observation
    with selected band pass.
    For use with converted Sky BG in photons."""


    #interpolate flux to 1A resolution on filter range
    interpFlux = interpolateAngstrom(pbWave, wave, flux)


    #calculated flux passed by filter
    modelflux = nansum(interpFlux*interpThroughput)


    return modelflux
```

```python
def magAB(fnu):
    """Calculate AB magnitude from flux in Fnu units."""
    return (-2.5*log10(fnu))-48.6


def modelMagnitude(pbWave,interpThroughput,wave,flux):
    """Model the magnitude of the observation
    with selected band pass.
    flux must be in fnu units.
    first two arguments are outputs
    from filter selection."""

    #model flux
    modelflux = modelFlux(pbWave,interpThroughput,wave,flux)

    #convert to AB mag
    return magAB(modelflux)
```

Bibliography

J. Anderson et al. Wide field camera 3 instrument handbook: 9.7 sky background. *STScI*, Chapter 9: WFC3 Exposure-Time Calculation, 2008.

S. Bowyer. The cosmic far ultraviolet background. *Annual review of astronomy and astrophysics*, 1991.

N. Byler. Nebular continuum and line emission in stellar population synthesis models. *arXiv:1611.08305*, 2016.

D. Calzetti. The dust content and opacity of actively star-forming galaxies. *The Astrophysical Journal*, 533(2), 2000.

G. Chabrier. Galactic stellar and substellar initial mass function. *Publications of the Astronomical Society of the Pacific*, 115(809), 2003.

C. Conroy, J. Gunn, and M. White. The propagation of uncertainties in stellar population synthesis modeling. i. the relevance of uncertain aspects of stellar evolution and the initial mass function to the derived physical properties of galaxies. *The Astrophysical Journal*, 699(1), 2009.

P. Côté. Wide field space astronomy study. Private Communication, 2018.

P. Côté et al. Castor: The cosmological advanced survey telescope for optical and ultraviolet research. Technical report, CSA, 2012.

P. Côté et al. Final report on the wide-field space astronomy study: The cosmological advanced survey telescope for optical and uv research (castor). Technical report, CSA, 2019.

B. Darvish. The effects of the local environment and stellar mass on galaxy quenching to z ˜ 3. *The Astronomical Journal*, 852(2), 2016.

T. Fellers and M. Davidson. *Concepts in Digital Imaging Technology: CCD Noise Sources and Signal-to-Noise Ratio*. Hamamatsu, 2019.

M. Giavalisco et al. New estimates of the sky background for the hst new estimates of the sky background for the hst exposure time calculator. Technical report, Space Telescop Science Institute, 2002.

I. Iwata. Quantum efficiency of the teledyne h2rg 2.5 micron cutoff detector. Private Communication, 2018.

J. Kartaltepe et al. A multiwavelength study of a sample of 70 micrometer selected galaxies in the cosmos field. i. spectral energy distributions and luminosities. *The Astrophysical Journal*, 2010.

J. Kruk et al. *Wide Field InfraRed Survey Telescope.* NASA, http://wfirst.gsfc.nasa.gov/, 2019.

P. Madau. Radiative transfer in a clumpy universe: The colors of high-redshift galaxies. *Astrophysical Journal*, 441(1), 1995.

C. Martin et al. *Galaxy Evolution Explorer.* JPL, http://www.galex.caltech.edu/, 2019.

Y. Mellier et al. *Euclid.* Euclid Consortium, http://www.euclid-ec.org/, 2019.

J. Murthy. Galex diffuse observations of the sky: The data. *The Astrophysical Journal Supplement Series*, 213(2), 2014.

M. Rafelski. Uvudf: Ultraviolet through near-infrared catalog and photometric redshifts of galaxies in the hubble ultra deep field. *The Astronomical Journal*, 150 (1), 2015.

C. Rodrigo et al. *The SVO Filter Profile Service.* Spanish Virtual Observatory, 2019.

M. Sawicki. Sedfit: Software for spectral energy distribution fitting of photometric data. *Astronomical Society Of The Pacific*, 2012.

R. Sorba and M. Sawicki. How future space-based weak-lensing surveys might obtain photometric redshifts independently. *Publications of the Astronomical Society of the Pacific, Volume 123, Issue 905*, 123(905), 2011.

R. Sorba and M. Sawicki. Missing stellar mass in sed fitting: spatially unresolved photometry can underestimate galaxy masses. *Monthly Notices of the Royal Astronomical Society*, 2015.

R. Sorba and M. Sawicki. Spatially-unresolved sed fitting can underestimate galaxy masses: a solution to the missing mass problem. *Monthly Notices of the Royal Astronomical Society*, 2018.

D. Spergel et al. Wfirst-2.4: What every astronomer should know. Technical report, California Institute of Technology, 2013.

C. Steidel et al. Spectroscopic confirmation of a population of normal star-forming galaxies at redshifts z ¿ 3. *Astrophysical Journal*, 1996.

B. Williams et al. The advanced camera for surveys nearby galaxy survey treasury. iv. the star formation history of ngc 2976. *The Astrophysical Journal*, 2010.